Insect Biochemistry and Molecular Biology 163 (2023) 104028

Contents lists available at ScienceDirect

Insect Biochemistry and Molecular Biology

journal homepage: www.elsevier.com/locate/ibmb

Insulin-like peptides and ovary ecdysteroidogenic hormone differentially stimulate physiological processes regulating egg formation in the mosquito *Aedes aegypti*

Kangkang Chen [1], Xiaoyi Dou [1], Jai Hoon Eum, Ruby E. Harrison, Mark R. Brown [**], Michael R. Strand [*]

Department of Entomology, University of Georgia, Athens, GA, USA

ARTICLE INFO

Keywords:
Insulin
Insulin-like growth factor
Ovary ecdysteroidogenic hormone
Ecdysone
Reproduction
Metabolism

ABSTRACT

Mosquitoes including *Aedes aegypti* are human disease vectors because females must blood feed to produce and lay eggs. Blood feeding triggers insulin-insulin growth factor signaling (IIS) which regulates several physiological processes required for egg development. *A. aegypti* encodes 8 insulin-like peptides (ILPs) and one insulin-like receptor (IR) plus ovary ecdysteroidogenic hormone (OEH) that also activates IIS through the OEH receptor (OEHR). In this study, we assessed the expression of *A. aegypti* ILPs and OEH during a gonadotrophic cycle and produced each that were functionally characterized to further understand their roles in regulating egg formation. All *A. aegypti* ILPs and OEH were expressed during a gonadotrophic cycle. Five ILPs (1, 3, 4, 7, 8) and OEH were specifically expressed in the head, while antibodies to ILP3 and OEH indicated each was released after blood feeding from ventricular axons that terminate on the anterior midgut. A subset of ILP family members and OEH stimulated nutrient storage in previtellogenic females before blood feeding, whereas most IIS-dependent processes after blood feeding were activated by one or more of the brain-specific ILPs and/or OEH. ILPs and OEH with different biological activities also exhibited differences in IIS as measured by phosphorylation of the IR, phosphoinositide 3-kinase/Akt kinase (AKT) and mitogen-activated protein kinase/extracellular signal-regulated kinase (ERK). Altogether, our results provide the first results that compare the functional activities of all ILP family members and OEH produced by an insect.

1. Introduction

Higher eukaryotes encode multiple insulin-like peptide (ILP) genes that are expressed as pre-pro-peptides with four domains (signal, B, C, and A) (Irwin, 2021; Shabanpoor et al., 2009). Vertebrate ILPs are subdivided into insulin that primarily regulates glucose uptake and intermediate metabolism, insulin-like growth factors (IGFs) that have mitogenic activities, and relaxins that have pleotropic functions (Bathgate et al., 2013; Belfiore et al., 2017; Haeusler et al., 2018). Insulins and relaxins are processed into separate B and A chains that are connected by two inter-disulfide bridges while IGFs have the same disulfide bridges but are processed into single peptides that retain the short C domain (Irwin, 202; Lawrence, 2021). Insulin binds a receptor tyrosine kinase (RTK) named the insulin receptor (IR) while IGFs preferentially bind related RTKs named IGFRs. Both activate signaling through the phosphoinositide 3-kinase/Akt kinase (PI3K/AKT) and mitogen-activated protein kinase/extracellular signal-regulated kinase (MAPK/ERK) pathways which together are known as insulin-IGF signaling (IIS). In contrast, relaxins signal through leucine-rich repeat containing G-protein coupled receptors (LGRs) (Bathgate et al., 2013; Patil et al., 2017).

Invertebrates like insects also encode multiple ILPs but their functional range is less understood (Álvarez-Rendón et al., 2023; Antonova et al., 2012; Chowański et al., 2021; Kannan and Fridell, 2013; Lin and Smagghe, 2019; Nässel et al., 2015; Semaniuk et al., 2021a, 2021b; Smýkal et al., 2020). This is due in part to most insects encoding only one IR/IGF-like RTK (usually named the IR), which makes it unclear how family members differentially regulate IIS-dependent metabolic and growth functions (Chowański et al., 2021; Nässel and Vanden

* Corresponding author.
** Corresponding author.
E-mail addresses: mrbrown@uga.edu (M.R. Brown), mrstrand@uga.edu (M.R. Strand).
[1] These authors contributed equally to this work.

https://doi.org/10.1016/j.ibmb.2023.104028
Received 24 September 2023; Received in revised form 12 October 2023; Accepted 23 October 2023
Available online 30 October 2023

Broeck, 2016; Semaniuk et al., 2021a; Vogel et al., 2013). One possibility is that within species, several ILP family members can bind and activate the IR but differences in downstream signaling result in variable physiological activities (Post et al., 2018). Differential expression or release could also contribute to family members within a given species having different physiological roles (Kim and Neufeld, 2015; Semaniuk et al., 2021b). However, it has also been noted that knockout of one or more ILP genes in *Drosophila* or mosquitoes either causes no defects in metabolic and/or growth activities or results in physiological alterations but no lethality due to potential redundancy among family members (Grönke et al., 2010; Liao and Nässel, 2020; Ling and Raikhel, 2018; Zhang et al., 2009). Producing ILPs that can be bioassayed independently provides another means for comparing the function of different family members but this approach is also difficult because these peptide hormones are more difficult to synthesize than many others due to their structure. As a result, only a few insect ILPs have been produced and bioassayed, while no study has produced and bioassayed all family members from the same species (Bai et al., 2012; Brown et al., 2008; Mizoguchi and Okamoto, 2013; Post et al., 2018; Wen et al., 2010).

Mosquitoes are insects of interest because many vector bloodborne pathogens including the causative agents of malaria, dengue fever, and yellow fever in humans (World Health Organization, 2014). Disease transmission only occurs through adult females that must blood feed on vertebrates to produce eggs (Clements, 2012). Egg formation in mosquitoes is also of interest from the perspective of ILP function because studies of the yellow fever mosquito, *Aedes aegypti*, indicate IIS regulates several activities during a gonadotrophic cycle (Roy et al., 2018; Strand et al., 2016). *A. aegypti* encodes 8 ILPs, 1 IR, and a putative relaxin receptor LGR4 (Brown et al., 2008; Ling et al., 2017; Ling and Raikhel, 2018; Sharma et al., 2019; Strand et al., 2016; Valzania et al., 2019). Seven family members (ILP1-5, 7 and 8) are processed into predicted insulin/relaxin-like hormones while ILP6 is processed into an IGF-like peptide (Brown et al., 2008; Riehle et al., 2006). Five family members (ILP1, 3, 4, 7, 8) are specifically expressed in the brain of adult females while three (ILP2, 5, 6) are preferentially expressed in other tissues (Riehle et al., 2006; Brown et al., 2008; Ling and Raikhel, 2021). ILP3 shares the highest amino acid identity with mammalian insulins but overall sequence homology is less than 50% as is the case for all ILPs produced by other insects (Brown et al., 2008; Nässel et al., 2015; Post et al., 2018). Most insects, including mosquitoes, additionally express a neuroparsin, unknown from vertebrates, named ovary ecdysteroidogenic hormone (OEH). *A. aegypti* OEH is expressed in brain medial neurosecretory cells and activates IIS but shares no sequence similarities with ILPs (Brown and Cao, 2001; Dhara et al., 2013; Vogel et al., 2015). We earlier produced synthetic *A. aegypti* ILP3 to demonstrate high affinity binding ($IC_{50} = 5.9$ nM) to the IR in ovary membranes (Wen et al., 2010) and later used a recombinant OEH to show that activity is unaffected by IR inhibition and demonstrate this hormone binds a different RTK named the OEHR (Valzania et al., 2019; Vogel et al., 2015).

A. aegypti females emerge in a previtellogenic state with primary follicles in the ovaries containing developmentally arrested oocytes (Valzania et al., 2019). Previtellogenic females consume sugar sources like nectar, which provision energy for flight and nutrients that are stored in the fat body as glycogen and neutral lipids (Baredo and DeGennaro, 2020; Briegel, 2003; Dou et al., 2023). Synthetic ILP3, recombinant OEH, and juvenile hormone (JH) upregulate enzymes with functions in glycogen and lipid synthesis while also stimulating nutrient storage (Brown et al., 2008; Dou et al., 2023; Hou et al., 2015; Wang et al., 2017; Zhu and Noriega, 2016). Primary follicles remain arrested until a female blood feeds, which activates the vitellogenic phase that culminates with development of oocytes into mature eggs that females lay. Ablating heads within 2 h of blood feeding inhibits the vitellogenic phase by ablating the source of brain-produced ILPs and OEH, whereas injection of ILP3 or OEH stimulates the ovaries to produce ecdysteroids that are converted to 20-hydroxyecdysone (20E) (Brown et al., 2008; Dhara et al., 2013). IIS and 20E signaling promote enzyme digestion of blood proteins and amino acid transport out of the midgut (Dou et al., 2023; Harrison et al., 2022; Roy et al., 2007). This bipartite signaling together with target of rapamycin kinase (TOR) signaling also stimulates vitellogenin (Vg) biosynthesis in the fat body that is concurrently dependent on mobilization of nutrient stores by adipokinetic hormone (Dou et al., 2023; Gulia-Nuss et al., 2011; He et al., 2021). Vg and other yolk components are then packaged into oocytes followed by chorion formation (Li and Li, 2006; Roy et al., 2018). Subsequent blood meals stimulate the same events, which enable females to produce multiple egg clutches over a lifespan (Harrison et al., 2021, 2022).

Taken together, previous findings suggest nutrient storage during the previtellogenic phase and the first step in the vitellogenic phase, ecdysteroid production by the ovaries, could depend solely on ILP3 and OEH. Alternatively, other ILP family members could also have functions in these or the other physiological processes that are required for egg development. In this study, we profiled the expression of all ILPs and OEH during a gonadotropic cycle. We then produced each ILP to use with OEH, 20E and JH in functional assays. We report that all ILPs and OEH are expressed during a gonadotropic cycle, as are the IR, OEHR and LGR4. Several ILPs and OEH stimulated nutrient storage in previtellogenic females, whereas tissue specific processes in the vitellogenic phase were primarily activated by ILPs and/or OEH expressed in the brain. Our results identify redundancy in the biological and signaling activity of some family members but distinct differences between others.

2. Materials and methods

2.1. Mosquitoes

The University of Georgia strain of *A. aegypti* (UGAL) was maintained as earlier described (Harrison et al., 2021). Females produced eggs for culture maintenance using defibrinated rabbit blood (Hemostat Laboratories) plus 1 mM ATP in warmed membrane feeders. For *in vivo* assays, females blood fed on an anesthetized rat. Handling and anesthetization of rats followed the protocol (A2020 12-008-R1) approved by The University of Georgia Institutional Animal Care and Use Committee, which maintains an Assurance of Compliance with the US Public Health Service and is accredited by the Association for Assessment and Accreditation of Laboratory Animal Care International and licensed by the US Department of Agriculture.

2.2. Synthetic ILP1-5, 7, 8, recombinant ILP6, and recombinant OEH

The genes encoding *A. aegypti* ILP1-5, 7 and 8 were previously examined to predict signal peptide and C chain enzymatic cleavage sites (Brown et al., 2008; Ling and Raikhel, 2021; Riehle et al., 2006) (Fig. S1A). The gene for ILP6 was predicted to encode two transcripts, *ilp6-A* and *ilp6-B*, that have signal peptides but no C chain enzymatic cleavage sites but RT-PCR data only detected *ilp6-B* in adults (Brown et al., 2008; Ling and Raikhel, 2021; Riehle et al., 2006) (Fig. S1A). OEH was also identified as a single chain peptide with a signal peptide (Vogel et al., 2015) (Fig. S1A). ILP1-5, 7 and 8 were synthesized in mg quantities (>80% purity) as complete or truncated B and A chains with canonical inter- and intrachain bonds between conserved Cys residues (CPC Scientific Inc; San Jose CA) using methods similar to earlier approaches used to synthesize ILP3 (Brown et al., 2008) (Fig. S1B). Synthesis of the B chains for ILP3 and ILP8 replaced the oxidation-prone methionine in each with a non-oxidizable norleucine (Fig. S1). Correct synthesis and disulfide bridge formation was assessed by confirming the molecular mass of each synthesized ILP by mass spectrometry (Table S2). ILP6-B was produced as a single chain recombinant protein in *E. coli* by isolating total RNA from adult females using Trizol reagent (Invitrogen) followed by cDNA synthesis and amplification of the entire coding region using specific primers with Ek/LIC overhangs (5′-GAC GAC GAC AAG ATA AGA GCC GTG CGA AAA TCA TG-3′ and 5′-GAG GAG AAG CCC GGT TTA GCA TTT ATT CTG TTG AAC TCC G-3′) and

iScript™ Reverse Transcription Supermix (Bio-Rad). The resulting cDNA was cloned into pET30 Ek/LIC (Novagen) in frame with N-terminal 6xHis- and S-tags, and a C-terminal His-tag, followed by expression in *E. coli* BL21a (DE3) cells that were grown in SOC medium (0.5% yeast extract, 2% tryptone, 10 mM NaCl, 2.5 mM KCl, 10 mM $MgCl_2$, 10 mM $MgSO_4$, 20 mM glucose) with 10 μg/ml of kanamycin to an optical density of 1.0 at 37 °C. Cells were then induced by adding isopropyl-β-d-thiogalactopyranoside (IPTG) to a final concentration of 0.1 mM, and grown as 800 ml cultures for 16 h at 16 °C. Bacterial cells were then harvested by centrifugation at 5000×*g* for 10 min followed by storage at −20 °C. Cell pellets were resuspended in lysis buffer (50 mM NaH_2PO_4, 300 mM NaCl, 10 mM imidazole) on ice for 1 h followed by addition of lysozyme (1 mg/ml) in 50 mM Tris buffer (pH 8.0) and sonication. After centrifugation of the lysate at 10,000×*g* for 25 min, supernatants were bound to a Ni-NTA matrix (5 Prime) pre-equilibrated with lysis buffer. Bound proteins were washed 5 × with wash buffer (50 mM NaH_2PO_4 300 mM NaCl, 20 mM imidazole) followed by elution with three column volumes of elution buffer (50 mM NaH_2PO_4, 300 mM NaCl, 40–300 mM imidazole). The eluted proteins from wash fractions were loaded onto 10% SDS-PAGE gels and visualized by Coomassie blue staining. Recombinant ILP6 (22,259 Da) eluted using 500 mM imadizole was desalted and concentrated by Centricon 10 (Millipore, USA) (Fig. S1B). Recombinant OEH (18,278 Da) used in the study was previously produced in *E. coli* and purified by HPLC (Vogel et al., 2015) (Fig. S1B).

2.3. ILP3 antibody, enzyme immunoassay, and immunocytochemistry

An antibody generated against *A. aegypti* ILP3 (Nuss and Brown, 2018) was assessed for recognition of ILP3 and other family members by enzyme immunoassay (EIA). In brief, ILP1-8 and OEH were solubilized in 90% acetonitrile with 0.1% trifluoroacetic acid as a 10 ng/100 μl stock. The top horizontal row of 96-well polystyrene microplates (Corning 3590) received 200 μl of each peptide in duplicate wells, and 100 μl from the wells was then transferred with a multi-tip pipettor into the lower rows containing 100 μl of the solvent to produce a 10 to 0.156 ng half step serial range for each of the peptides. Wells with solvent and no peptide were included for absorbance background controls. Plates were frozen and lyophilized overnight. For the following steps, all solutions were added as 100 μl/well. Wells were blocked with 1.5% bovine serum albumin (BSA) in phosphate buffered saline (PBS) (Na_2HPO_4 10 mM, KCl 2.7 mM, NaCl 137 mM and KH_2PO_4 1.8 mM, pH7.4) for 1–2 h at room temperature (RT). Wells were then cleared, rinsed once with PBS containing 0.2% Tween 20 (PBST), and cleared again before adding AaILP3 rabbit polyclonal antibody (3580 production bleed, 1:2000 in PBS plus 1.5% BSA (Nuss and Brown, 2018). Plates were sealed and held overnight in a humid chamber at 4 °C with no agitation. Wells were cleared, rinsed two times with PBST, and treated with peroxidase-conjugated goat anti-rabbit IgG antibody (1:7000; Jackson Laboratories) in 1.5% BSA PBS at RT for 4 h as above. Wells were cleared, rinsed with two changes of PBST, and treated with substrate (3, 3′,5,5′-tetramethylbenzidine; KPL 50-76-00) for 15 min in the dark at RT. Addition of 0.5 M phosphoric acid stopped the reaction, and absorbance values/well recorded with a plate reader at 450 nm (BioTek MQX200).

For immunocytochemistry, brains and digestive tracts were dissected in PBS from 4-day old previtellogenic females before blood feeding (=non-blood fed (NBF)) and 4-day old females 6 h and 48 h after consuming a blood meal (=post-blood meal (PBM)). Females were placed at 4 °C for 3–5 min and then dissected in ice-cold PBS. Heads were carefully removed from the body by cutting at the neck with sharp scissors under a dissecting microscope. The whole gut was also explanted from the decapitated female using forceps. Heads were placed in ice-cold fixative (3% NaCl, 0.25% Triton X100 and 4% paraformaldehyde in PBS) and fixed for 3 h on a rocker in a cold room. Guts were placed in fixative (4% paraformaldehyde in PBS) for 30 min on a rocker at room temperature. Fixed heads were put on ice and dissected to collect intact brains using forceps. Brains and guts were washed 3x in PBS before permeabilizing in 4% paraformaldehyde in PBS containing 0.5% Triton X 100 for 30 min, washing 3x (5 min each) in 1 ml PBS containing 0.2% Tween 20 (PBT) on a rocker at RT, and blocking in 2.5% BSA in PBT on a rocker at RT for 1 h. Brains and guts were then incubated with anti-ILP3 (1:50, affinity purified 3580 Ew2+3) or a previously generated anti-OEH (1:2000) (Brown and Cao, 2001) for 2 days on a rocker at 4 °C. After washing 3x in PBS, an Alexa Fluor 488 secondary antibody (1:2000; Thermo Fisher Scientific) was added and incubated in darkness for 1 day on a rocker at 4 °C. Samples were then rinsed again 3x in PBS and mounted on slides in 50% glycerol in PBS. Samples were examined using a Leica epifluorescence microscope fitted with a digital camera. Resulting images were exported to Adobe Photoshop. Relative abundance of ILP3 per medial neurosecretory cell (mNSC) or ventral nerves on the midgut was assessed by measuring pixel intensity using ImageJ software (National Institutes of Health, Bethesda, MD, USA) which calculates pixel intensity in arbitrary units. For each treatment, pixel intensities were measured in a minimum of 9 mNSCs and ventral nerve groups from 10 females using captured images that were acquired under identical exposure and gain conditions with background subtracted (https://imagej.nih.gov/nih-image/manual/tech.html).

2.4. Quantitative reverse transcriptase (qRT-)PCR

Gene specific primers were synthesized by IDT (Integrated DNA Technologies for the following *A. aegypti* genes: *ir*, *oeh*, *oehr*, *lgr4*, and *ilp1-8, vitellogenin A1* (*AaVgA1*), *serine protease VI* (*AaSPVI*), chorion protein *15a3* (*Aa15a3*), and ribosomal protein 8 (*rpl8*) (normalizing control) (Table S1). The homolog of *A. aegypti* LGR4 is the predicted relaxin-like receptor for *D. melanogaster* ILP7 while a second LGR designated as LGR3 is the predicted receptor for *D. melanogaster* ILP8 but has no homolog in *A. aegypti* (Veenstra, 2020). The two other *lgr* genes in the *A. aegypti* genome were recently deorphanized as the glycoprotein GPA2/GP5B receptor (LGR1, AAEL004399) and bursicon receptor (LGR2, AAEL004777) (Veenstra, 2020). Newly emerged previtellogenic females were provided *ad libitum* access to a sugar solution and water until 4 days post-emergence (PE) and then blood-fed. Females were then sampled immediately before blood feeding (0 h) or 2, 6, and 24 h PBM when head with brain, gut (fore-, mid-, and hindgut), ovaries and remaining abdomens (=pelt) containing fat body, epidermis and ventral nerve chord were collected by dissection in PBS. Each biological replicate consisted of the above organs or tissues from two females with at least three biological replicates analyzed per treatment and time point. For all samples, total RNA was extracted using TRIzol (Ambion) according to the manufacturer's instructions followed by reverse transcription of a 1 μg sample using a cDNA synthesis kit (Bio-Rad). Relative expression of each ILP family member and OEH was assessed by qRT-PCR and the $2^{-(\Delta\Delta CT)}$ method (Livak and Schmittgen, 2001) with data normalized to *rpl8* (Dzaki et al., 2017). Quantitative estimates of transcript abundance were determined for the *ir, oehr,* and *lgr4* by dissecting 4-day old previtellogenic females (NBF), and 2, 6 and 24 h PBM females in PBS and collecting tissue samples, isolating total RNA and synthesizing cDNA templates as described above. cDNA from the ovaries was used to amplify a portion of each target gene using specific primers (Table S1) followed by cloning into TOPO TA 2.1 (Invitrogen). After transformation into NEB-10β competent *E. coli* (NEB), plasmid DNA was extracted using a GeneJET Plasmid Miniprep Kit (Thermo) and each insert sequenced (Psomagen) to confirm identity. Serial dilutions of 10^3-10^8 plasmid copies were used to generate a standard curve which was then used to estimate transcript abundance of each target gene in the different samples using established methods (Dou et al., 2023). qRT-PCR data were generated from each tissue and treatment using the QuantiFast SYBR Green PCR Kit 4000 (Qiagen), run in quadruplicate technical replicates on a Rotor-Gene Q cycler (Qiagen) under the

following conditions: initial denaturation at 95 °C for 10 min, followed by 35 cycles of which denaturation at 95 °C for 10 s, annealing at 55 °C for 15 s, and extension at 72 °C for 20 s. A minimum of three independently collected biological samples were collected and analyzed for each treatment and time point.

2.5. Triacylglycerol and glycogen assays

To assess triacylglycerol (TAG) and glycogen stores in response to different hormones, one cohort of 4-day old NBF females were sugar fed, injected with each ILP or OEH (20 pmol in 0.5 μl saline), 20E (100 ng (=210 pmol)) in 0.5 μl saline, Sigma) or saline and immediately decapitated. A second cohort of 4-day old females was topically treated with methoprene (Zoecon) (250 ng (=800 pmol) in 0.25 μl of ethanol) and immediately decapitated. Abdomen pelts containing the fat body but with the gut and ovaries removed were then collected by dissection in PBS 24 h later. Each biological sample used to measure TAG and glycogen stores for a given treatment consisted of two abdomen pelts that were homogenized in 100 μl of PBS containing 0.5% Tween-20 and then incubated at 70 °C for 5 min. Pelt samples were centrifuged at 3000×*g* for 1 min and 15,900×*g* for 3 min followed by transfer of 10 μl from each sample to individual wells of 96-well plates (Corning). After adding 100 μl of TAG reagent (Thermo-Fisher) and gentle mixing, samples were incubated for 10 min at room temperature and absorbance was measured with a Synergy plate reader (BioTek) at 530 nm. A range of TAG standards (MedTest Dx, Canton MI) was included in the wells of each plate and used to calculate experimental values from a regression line. Glycogen levels were measured using a Glycogen Assay Kit (Cayman) per instructions from the manufacturer. Briefly, two pelts were homogenized in 100 μl diluent assay buffer and then centrifuged at 3000×*g* for 10 min. Sample supernatants (10 μl) were transferred to wells in 96 well plates followed by hydrolysis enzyme solution (50 μl) for a 30 min incubation at 37 °C and then developer solution (150 μl) for 15 min at 37 °C. Plate wells were read with the same instrument as above with an excitation wavelength of 530 nm and an emission wavelength of 585 nm. Glycogen standards in wells of the same plate were similarly set up and read to calculate experimental values as above.

2.6. Ovary ecdysteroid production

Triplicate sets of two pairs of ovaries from 4-day old previtellogenic females (NBF) were placed into 60 μl of Sf900 II (Gibco) in a 0.6 ml microtube cap followed by addition of 2 and 20 pmol of ILP1-8 or OEH in 6 h at 27 °C. The caps were placed in a 24 well plate with a drop of water in each well, covered, and gently rocked in a box suspended in a water bath to maintain a constant high humidity. After incubation, media containing secreted ecdysteroids were individually collected and frozen. Ecdysteroid content in each sample (25 μl of the collected volume/well) was determined by enzyme-linked immunoassay (EIA) using the EAB27 rabbit antibody, which recognizes 20E and ecdysone equally, and calculated from a semi-log linear regression line of 20E standards (4–2000 pg, Millipore Sigma) and corrected for amount secreted by one ovary pair (McKinney et al., 2017).

2.7. Yolk deposition into oocytes

Newly emerged females were provided *ad libitum* access to 10% sucrose for 2 days post-emergence (PE), followed by water only on day 3 PE, and blood fed to repletion on day 4 PE on an anesthetized rat for 5 min. Replete females were decapitated within 1 h PBM and injected with each ILP family member (20 pmol per female) OEH (20 pmol), or 20E (500 ng (=1 nmol)) in saline (0.5 μl per female), which similar to the TAG and glycogen assays described above was administered at a higher dose than in *ex vivo* assays due to presumptive metabolism (Brown et al., 2008; Dou et al., 2023; Gulia-Nuss et al., 2011; Harrison et al., 2022). Intact (non-decapitated), blood-fed females injected with saline served as a positive control while decapitated females injected with saline served as the negative control. Ten or more females were injected for each treatment and held in small containers in the above rearing conditions. At 36 h PBM, ovaries from each female were dissected and examined by measuring the length of yolk deposition (mm) along the anterior-posterior axis of five oocytes with the average length serving as the yolk deposition value for each female (Brown et al., 2008; Harrison et al., 2021).

2.8. AaVgA1, AaSpVI, and Aa15a3 expression assays

Two abdominal pelts or two pairs of ovaries were dissected from 4-day old previtellogenic females in PBS and floated on 59 μl of Sf900II medium in a 0.5 ml microtube cap. Two whole guts were dissected from newly blood fed four-day old females and similarly set up in *ex vivo* cultures as above. Each ILP (20 pmol) or OEH (20 pmol) in 1 μl of saline was added individually or with 20E (6 pmol) to cultures for 6 h at 28 °C. Total RNA was then extracted from each tissue, cDNA synthesized, and qRT-PCR reactions run using specific primers (Table S1) to amplify transcripts for the *A. aegypti vitellogenin A1* (*AaVgA1*, U02548), *serine protease VI* (*AaSPVI,* GQ398048), or *chorion protein 15a3* (*Aa15a3*, AAEL014561) as described above. Each amplicon was also cloned into pCR2.1 (Invitrogen) and transformed into NEB-10β (NEB). Plasmids were extracted using GeneJET Plasmid Miniprep Kit (Thermo) and sequenced. Serial dilutions of 10^3-10^8 plasmid copies were used to generate a standard curve which was then used to estimate transcript abundance of each target gene in the different experimental samples. qRT-PCR data were generated as described above, run in quadruplicate technical replicates on a Rotor-Gene Q cycler (Qiagen) under the following conditions: initial denaturation at 95 °C for 10 min, followed by 35 cycles of which denaturation at 95 °C for 10 s, annealing at 55 °C for 15 s, and extension at 72 °C for 20 s. A minimum of three independently collected biological samples were collected and analyzed for each treatment and time point. To determine whether IR signaling was required for upregulated expression of *Aa15a3*, the IR inhibitor, OSI-906 (10 mM stock in DMSO) was added to cultures at 170 and 850 nM along plus ILP3 (20 pmol) and 20E (6 pmol). The same concentration of DMSO without inhibitor served as the negative control.

2.9. Immunoblotting

Five pairs of ovaries, five whole guts (fore-, mid-, and hindgut), or 3 abdomen pelts containing fat body with gut and ovaries removed were dissected from 4-day old previtellogenic female and placed into 59 μl of Sf900II medium in a 0.5 ml microfuge cap followed by addition of 20 pmol of ILP2, 3, 5, 7 or OEH for 1 h (ovaries, pelts) or 3 h (guts) bringing the final volume up to 60 μl. The negative control was incubation of each organ in medium only. PRO-PREP extraction solution (100 μl; 17,081 Intron Biotechnology) with 1 X protease and phosphatase inhibitors (Thermo Fisher Scientific) was added to each sample and homogenized using the MP Biomedical Fastprep 24 Sample Preparation System. Protein concentration was determined using Coomassie Plus Protein reagent (Thermo Fisher Scientific). Samples were mixed with 4x Laemmli buffer containing 10% mercaptoethanol, boiled for 5 min, and electrophoresed (50 μg per lane) on 4–20% Trish-HCl gels (Bio-Rad), followed by transfer to polyvinyl difluoride (PVDF; Thermo Fisher Scientific). After blocking in 5% nonfat dry milk in PBS buffer with 0.05% Tween 20 (PBST), the blots were sequentially probed overnight with primary antibodies to phosphorylated IR (pIR) (1:1000, 3024 S, Cell Signaling Technology), pAKT (Thr342) (1:1000, p104-342, PhosphoSolutions), pERK (1:1000, 4370 S, Cell Signaling Technology), or actin (1:2000, A2103, Sigma-Aldrich) which was used as a loading control with prior evidence confirming each primary antibody visualizes the phosphorylated form of the target protein but not the non-phosphorylated form in *A. aegypti* (Martinson et al., 2022; Valzania et al., 2018, 2019). Blots were washed 3 times with PBST and probed with a

peroxidase-conjugated goat anti-rabbit secondary antibody (1:5000, Jackson Labs) for 2 h. After 3 times wash with PBST, blots were visualized using a chemiluminescent substrate (Clarity, Bio-Rad) and a Syngene imaging system. Each blot was then stripped and probed with another primary antibody and processed until all targets were visualized. Each treatment was examined in triplicate using independently collected samples. Relative abundance of pIR, pAKT and pERK was estimated by measuring pixel intensity using ImageJ. For each treatment, pixel intensities were measured for each treatment band relative to the actin loading control using captured images that were acquired under identical exposure and gain conditions (https://imagej.nih.gov/nih-image/manual/tech.html).

2.10. Data analysis

All data sets were analyzed using JMP Pro 16.0 (SAS, Cary, NC). Data sets were first analyzed for being normally distributed using a Shapiro-Wilk test or Bartlett's homogeneity of variances test followed by either one-way ANOVA and a Tukey-Kramer least significant difference test, one-way ANOVA and a Dunnetts test that compared each treatment to a

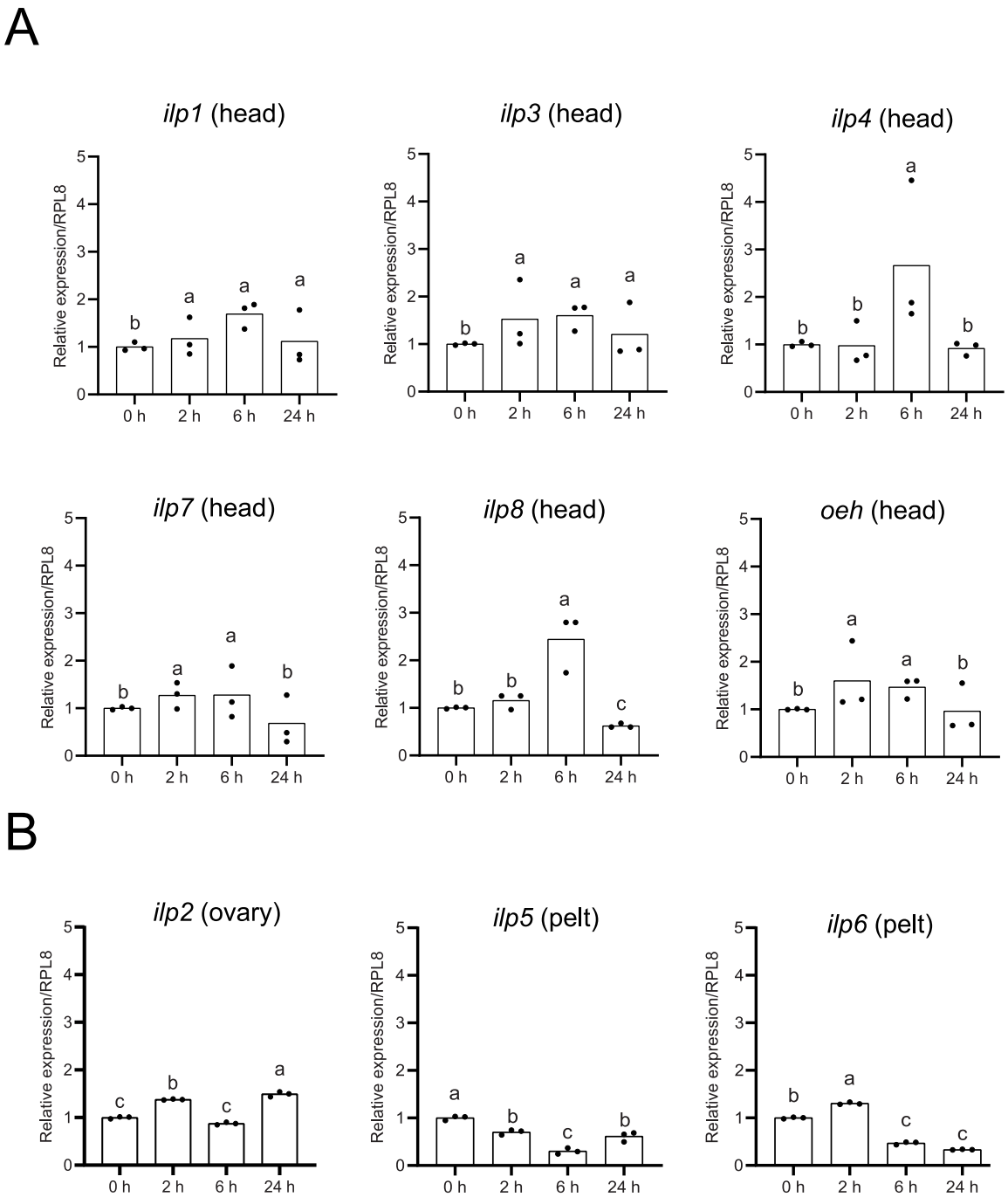

Fig. 1. Relative expression of most *ilp* genes and *oeh* increases after blood feeding. (A) Brain-specific ILPs (*ilp1, 3, 4, 7, 8*) and *oeh.* (B) ILPs preferentially expressed in other tissues (*ilp2, ilp5,* and *ilp6*). Data for *ilp2* come from the ovaries while data for *ilp5* and *ilp6* come from pelts. Relative transcript abundances were normalized to the reference gene *rpl8* with different letters above a given bar indicating fold change significantly differed (Tukey-Kramer post-hoc multiple comparison test; $P \leq 0.05$). Each bar shows treatment means while solid circles show values for the three independently collected biological replicates that were analyzed for each treatment and time point.

designated control, or a non-parametric Kruskal-Wallis test followed by a Dunn's test with a designated control. Figures were generated using GraphPad Prism 10.0 that were exported to Adobe Illustrator.

3. Results

3.1. Most ILPs and OEH are expressed in the brain while receptors are expressed globally

Consistent with earlier findings (Riehle et al., 2006; Brown et al., 2008; Ling et al., 2017), qRT-PCR assays specifically detected transcripts for *ilp1, 3, 4, 7, 8*, and *oeh* in the head (Fig. S2). *ilp5* and *ilp6* were exclusively or preferentially detected in the pelt containing fat body, epidermis and ventral nerve chord, while *ilp2* was preferentially detected in the in the ovaries (Fig. S2). After blood feeding, relative abundance of all brain-specific ILP family members and *oeh* increased by 6 h PBM and either remained elevated or declined by 24 h PBM to similar levels in previtellogenic (NBF), 4-day old females (=0 h) (Fig. 1A). We noted that *ilp6* in the pelt and *ilp2* in the ovaries also increased after blood feeding, whereas *ilp5* in the pelt declined (Fig. 1B). Profiling transcript copy number for the *ir*, *oehr* and *lgr4* in previtellogenic, 4-day old females detected each in the ovary, gut, pelt, and head (Fig. S3). Transcript abundances for the *ir* and *oehr* were much higher in the ovaries than other tissues, and also were higher than *lgr4* in all tissues (Fig. S3). After blood feeding, *ir* abundance further increased in the ovaries and head by 24 h PBM but not in the pelt and gut (Fig. S4). Copy number for *oehr* increased in the ovaries by 2 h PBM and in the head by 24 h PBM while largely remaining unchanged in the pelt and gut (Fig. S4). Copy number for *lgr4* also increased in the ovaries after blood feeding but not in other tissues (Fig. S4). Taken together, transcripts for all ILP family members, OEH and their candidate receptors were expressed during the previtellogenic and vitellogenic phases of the first gonadotropic cycle.

3.2. Blood feeding stimulates ILP3 and OEH release from ventricular nerves

An antibody generated to ILP3 recognized this family member but no others in an EIA (Fig. S5). This antibody specifically detected ILP3 in brain medial neurosecretory cells (mNSCs) but no difference in labeling intensity was detected between previtellogenic NBF 4-day old females, 6 h PBM females and 48 h PBM females (Fig. 2A and D). Thus, transcript abundance increased in the head after blood feeding but labeling of ILP3 in mNSC cell bodies did not. Axons from mNSCs radiate out of the brain

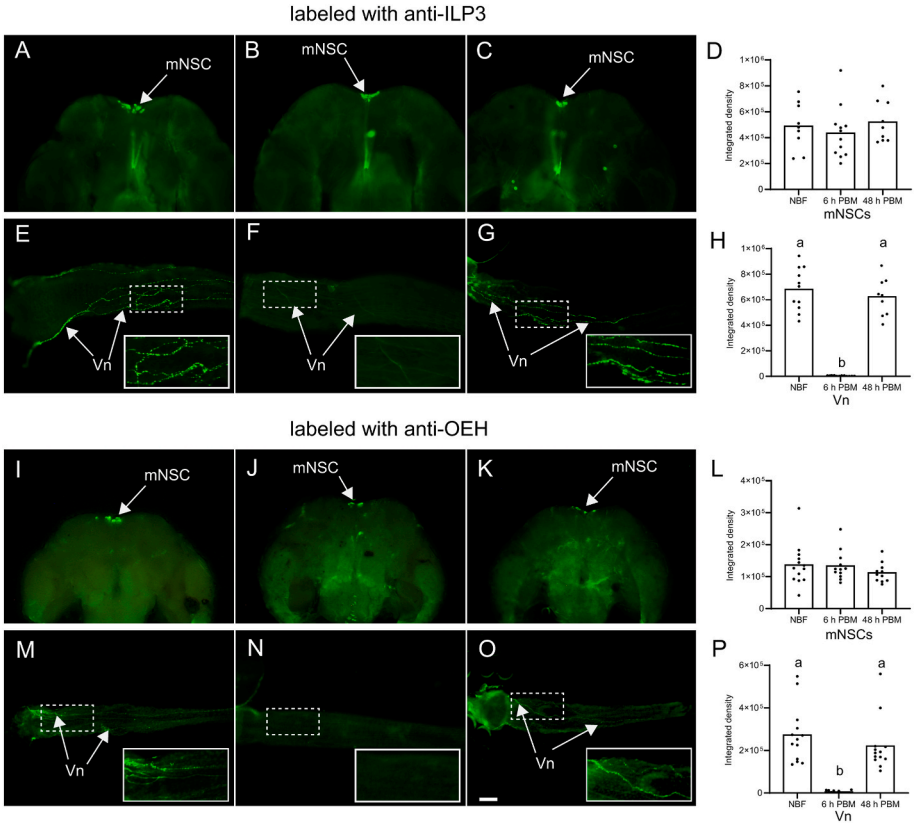

Fig. 2. ILP3 and OEH location and release. ILP3 (A–H) and OEH (I–O) are specifically detected in brain medial neurosecretory cells (mNSCs) and markedly decrease in ventricular nerves after blood feeding. Epifluorescence microscopy images of mNSCs in brains from 4-day old females that were labeled with anti-ILP3 (green): (A) before blood feeding (NBF), (B) 6 h PBM, and (C) 48 h PBM. (D) Quantification of ILP3 in mNSCs at each sample time in arbitrary pixel intensity units. No significant difference was detected between treatments (One-way ANOVA; $P \geq 0.05$). Epifluorescence microscopy images of anterior midguts from 4-day old females labeled with anti-ILP3 (green): (E) before blood feeding (NBF), (F) 6 h PBM, and (G) 48 h PBM. Ventricular nerves (Vn) radiating from mNSCs are strongly labeled by anti-ILP3 in (E) and (G) but not (F). Hatched box in each image corresponds to the insert showing the ventricular nerve at higher magnification. (H) Quantification of ILP3 in ventricular nerves at each sample time in arbitrary pixel intensity units. ILP3 labeling was significantly higher in NBF and 48 h PBM females than in 6 h PBM females (ANOVA followed by a Tukey-Kramer post-hoc test with different letters above each bar indicating treatments that differed; $P \leq 0.001$). (I–K) Epifluorescence microscopy images of mNSCs at the same time points as A-C but stained with anti-OEH. (L) Quantification of OEH in mNSCs at each sample time in arbitrary pixel intensity units. No significant difference was detected between treatments (ANOVA; $P \geq 0.05$). (M–O) Epifluorescence microscopy images of ventricular nerves on the anterior midgut at the same time points as E-G but stained with anti-OEH. Hatched boxes and inserts in M-O are also the same as in E-G. Quantification of OEH in ventricular nerves at each sample time in arbitrary pixel intensity units. OEH labeling was significantly higher in NBF and 48 h PBM females than in 6 h PBM females (One-way ANOVA followed by a Tukey-Kramer post-hoc test; $P \leq 0.001$). Scale bar in O equals 75 mm with all other images being at the same magnification.

as 2 pairs of nerves (nervi corporis cardiaci (NCC) I and NCC II) that merge to form corpus cardiacum (CC) over the aorta in *A. aegypti* (Clements et al., 1985; Meola and Lea, 1972). The axons then extend along with the stomatogastric nerves from the hypocerebral ganglion to form ventricular nerves that terminate along the anterior midgut (Brown and Cao, 2001; Cao and Brown, 2001). Anti-ILP3 strongly labeled the ventricular nerves in previtellogenic 4-day old females, but signal intensity was strikingly lower at 6 h PBM before returning to previtellogenic levels at 48 h PBM (Fig. 2E–H). Anti-OEH also strongly labeled mNSC cell bodies with no difference in labeling intensity between NBF, 6 h PBM and 48 h PBM females, whereas signal in ventricular nerves was also much lower at 6 h PBM before returning to NBF levels at 48 h PBM (Fig. 2I-P). These results strongly suggested blood feeding stimulates a rapid release of ILP3 and OEH from axons on the anterior midgut after blood feeding which was followed by peptide restoration by the end of the vitellogenic phase (48 h PBM) when mature eggs have developed (Harrison et al., 2021; Valzania et al., 2019).

3.3. Several ILPs and OEH stimulate nutrient storage during the previtellogenic phase

As earlier noted, sugar feeding by previtellogenic females provides nutrients that are stored in the fat body as neutral lipids like TAG and glycogen (Brown et al., 2008). The importance of these nutrient stores to the vitellogenic phase is supported by results showing that 80% of the lipids in mature eggs produced in the first gonadotropic cycle derive from sugar consumed during the previtellogenic phase (Ziegler and Ibrahim, 2001). However, prior studies also show that head ablation after sugar feeding inhibits the increase in nutrient stores, while ILP3 dose-dependently increases stores to similar levels as intact (non--decapitated) females (Brown et al., 2008). To assess whether this activity was restricted to ILP3, we conducted the same bioassay by injecting a 20 pmol dose of the other *A. aegypti* ILP family members or OEH in saline. Decapitated females topically treated with methoprene (800 pmol) or injected with a single dose of 20E (210 pmol) were also included given evidence the former also promotes nutrient storage while the latter is required for the vitellogenic phase when nutrient stores are mobilized (Dou et al., 2023; Wang et al., 2017). TAG in pelts from intact females or decapitated females treated with ILP3, ILP7, ILP8 and OEH were higher than in control females that were decapitated and injected with only saline (Fig. 3A). Likewise, glycogen was also higher in intact females and decapitated females treated with ILP1, ILP2, ILP3, OEH and methoprene when compared to control females (Fig. 3B).

3.4. Brain-specific ILPs and OEH stimulate ovaries to produce ecdysteroids

Head-ablation within 2 h of blood feeding inhibits initiation of the vitellogenic phase as indicated by low production of ecdysteroids by the ovaries (Brown et al., 2008; Dhara et al., 2013). We thus tested whether other ILP family members also stimulate ecdysteroid production by the ovaries using an established *ex vivo* assay where ovary pairs from 4-day old previtellogenic females are incubated for 6 h in Sf900 II medium plus 2 pmol or 20 pmol of each ILP, OEH, or no added hormone. We then measured ecdysteroids in the medium by EIA (McKinney et al., 2017). Only ILP3 stimulated a significant increase in ecdysteroids when 2 pmol of each hormone was added, whereas all of the brain-specific ILPs (ILP1, 3, 4, 7, 8) and OEH stimulated an increase in 20E when 20 pmol was added (Fig. 4). In contrast, adding 20 pmol of ILP2, 5 and 6 that are expressed in other tissues did not stimulate the ovaries to increase ecdysteroid production (Fig. 4).

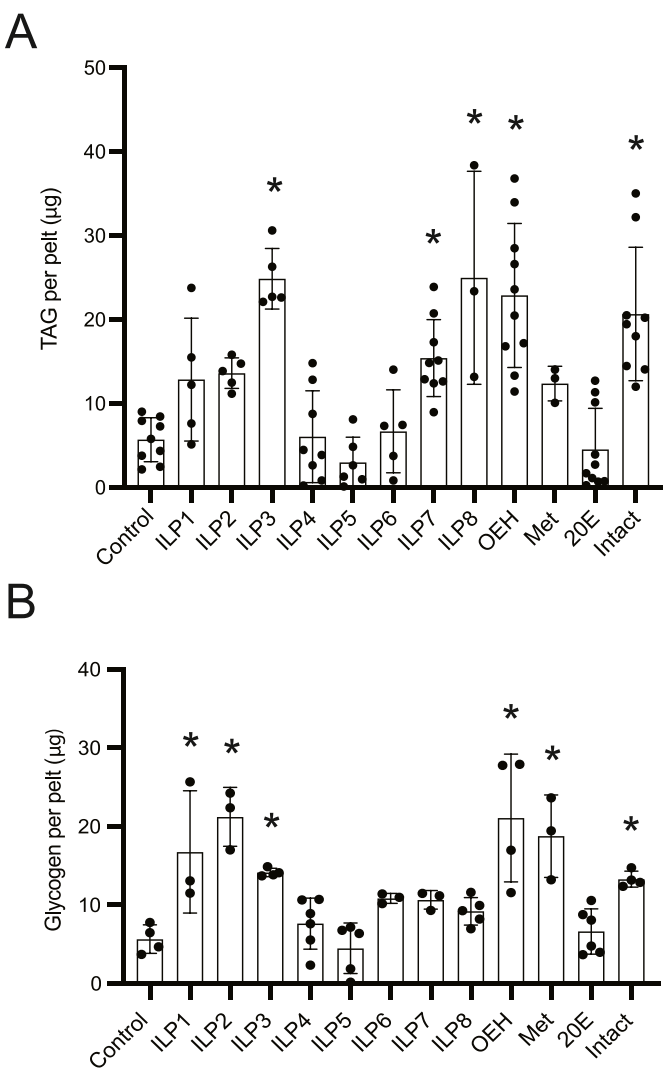

Fig. 3. Hormone effects on nutrient stores. Hormones with functions in regulating a gonadotrophic cycle in *A. aegypti* differentially affect nutrient stores in the fat body of 4-day old previtellogenic females after sugar feeding. Females were decapitated immediately after sugar feeding and injected with saline (Control), ILP1-8 (20 pmol), OEH (20 pmol) or 20E (200 pmol), or topically treated with methoprene (Met) (800 pmol). Intact females were sugar fed but not decapitated. (A) TAG stores 24 h post-treatment. (B) Glycogen stores 24 h post-treatment. Each bar shows treatment means ± standard deviation (SD) while solid circles indicate values for individual biological replicates. For each graph, an asterisk above a bar indicates that TAG or glycogen amount significantly differ from the control while no asterisk indicates the treatment did not differ (Dunnett's post-hoc multiple comparison test; $P \leq 0.05$). A minimum of three and a maximum of ten independently collected biological replicates were analyzed for each treatment.

3.5. Head-produced ILPs and OEH plus 20E stimulate AaVgA1 expression in the fat body, AaSPVI expression in the midgut and AaCP-15a3 expression in the ovaries

20E, TOR signaling and IIS interact to activate expression of Vg genes such as *AaVgA1* in the fat body and serine protease genes like *AaSPVI* in the midgut that digest blood proteins (Dou et al., 2023; Gulia-Nuss et al., 2011; He et al., 2021; Isoe et al., 2009; Roy et al., 2007). We thus conducted *ex vivo* assays with dissected abdominal pelts containing the fat body in the same medium used for ovaries which provides amino acids that activate TOR signaling (Gulia-Nuss et al., 2011; Valzania et al., 2019). Individually adding each ILP (20 pmol), OEH (20 pmol) or

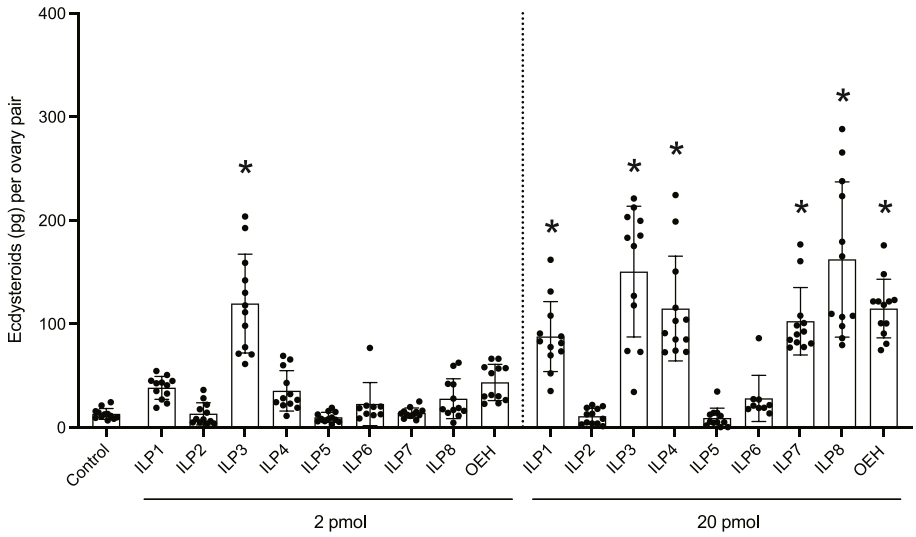

Fig. 4. ILPs and OEH differentially stimulate ecdysteroid production by ovaries. Ovaries from two 4-day old previtellogenic females were placed in Sf900 medium alone (Control), or Sf900 medium plus 2 pmol or 20 pmol of each ILP or OEH. Ecdysteroids in the medium were measured 6 h post-treatment. Each bar shows treatment means ± standard deviation (SD) while solid circles indicate values for individual biological replicates. An asterisk above a bar indicates ecdysteroids significantly differed from the control while no asterisk indicates that treatment did not differ (Dunnett's post-hoc multiple comparison test; $P \leq 0.05$).

20E (10 pmol) alone to cultures resulted in no increase in *VgA1* copy number, whereas copy number increased when each of the brain-specific ILPs, except ILP7, plus 20E were added together (Fig. 5A). The same assay using whole guts dissected from 4-day old females within 1 h of blood feeding similarly showed no increase in *AaSPVI* copy number when each ILP, OEH or 20E was added alone (Fig. 5B). Treatment with most of the ILPs and OEH in the presence of 20E trended to increase copy number of *AaSPVI* when compared to the negative control, but only ILP4 plus 20E was statistically significant due to variability among replicates for the other treatments (Fig. 5B). Following yolk packaging into oocytes, follicle cells secrete a chorion that results in mature eggs females fertilize and lay (Harrison et al., 2021; Li and Li, 2006; Valzania et al., 2019). No studies had previously assessed whether ILPs, OEH, and/or 20E affect chorion gene expression but we tested this by adding ILPs, OEH and 20E alone or together to ovary cultures followed by measuring copy number of *Aa15a3* that encodes a major *A. aegypti* chorion protein (Li and Li, 2006). No ILP (20 pmol), OEH (20 pmol) or 20E (10 pmol) alone stimulated increased *Aa15a3* copy number, whereas four of the brain-specific ILPs and OEH plus 20E did so (Fig. 5C). To confirm the specificity of ILP action, we added two concentrations of the IR inhibitor OSI-906 to ovary cultures containing ILP3 plus 20E that previous studies had shown to dose-dependently inhibit ecdysteroid synthesis (Dhara et al., 2013; Valzania et al., 2019). Consistent with expectation from prior results, the higher concentration of OSI-906 we used in these assays (850 nM) inhibited the increase in copy number of *Aa15a3* that occurred when ovaries were treated with ILP3 plus 20E (Fig. S6). Thus, all of the brain-specific ILPs except ILP7 activated downstream processes in the ovaries, fat body and midgut required for egg maturation after blood feeding but only in combination with 20E which alone did not increase transcript abundance of *VgA1, AaSPVI* or *Aa15a3* when compared to the saline only control treatment.

3.6. Most ILPs, OEH and 20E stimulate yolk deposition into oocytes

Yolk deposition into oocytes is completed by 48 h PBM which is followed by follicle cells secreting a chorion. Yolk deposition does not occur in *ex vivo* ovary assays because it depends on both the fat body and transport molecules in the hemolymph (Sun et al., 2000). However, previous results showed that decapitating females within 2 h of blood feeding fully inhibits yolk deposition, while a single 10 pmol dose of ILP3 or OEH restored it to levels that were only slightly lower than in control (non-decapitated) females (Brown et al., 2008). Since only the head specific ILPs stimulated *VgA1* expression, we expected that only these would stimulate yolk deposition when injected into decapitated females but results showed that all family members except ILP5 stimulated the same level of yolk deposition as OEH and 20E (Fig. 6).

3.7. ILPs differentially stimulate phosphorylation of IR, AKT and ERK

We assessed whether biological activity of ILPs used in the preceding functional assays correlated with activating IIS as measured by detection of pIR, pAKT and pERK on immunoblots using antibodies that recognize each in *A. aegypti* (Martinson et al., 2022; Valzania et al., 2018, 2019). We first used ILP3, which stimulated most of the physiological processes we measured in the preceding assays to conduct a time course assay. Adding 20 pmol of ILP3 to *ex vivo* ovary, pelt and gut cultures resulted in detection of pIR, pAkt and pERK in ovaries and pelts at 20 min which was sustained to 3 h before declining at 6 h (Figs. S7A and B). In gut samples, pIR and pAkt were weakly detected at 20 min and 1 h before increasing at 3 and 6 h, while pERK was detected without addition of ILP3 (Fig. S7C). Based on these patterns, we compared signaling between family members by comparing ILP3 to ILP2 and ILP7, which exhibited more restricted activity in the preceding assays, and ILP5 which showed no activity. Twenty pmol of each hormone was added to ovary and fat body cultures for 1 h and guts for 3 h. In ovaries, ILP3 stimulated an increase in pIR, pAKT and pERK, ILP7 stimulated an increase in pIR and pERK, ILP2 stimulated an increase in pERK only, and ILP5 had no effect (Fig. 7A). In pelts, ILP3 and ILP7 stimulated an increase in pIR and pAKT, ILP2 stimulated a small increase in pAKT, while ILP5 had no effect (Fig. 7B). In guts, ILP3 also stimulated an increase in pIR and pAKT, but ILP7 only stimulated an increase in pAKT, while ILP2 and ILP5 showed no activity (Fig. 7C). Unlike ovaries, pERK was detected in both the fat body and gut in control samples where no ILP was added (Fig. 7B and C). We also analyzed IIS after adding 20 pmol of OEH to ovary, pelt and gut cultures. In ovaries, OEH increased pAKT and pERK but did not increase pIR (Fig. 8A), which was consistent with prior results indicating this hormone binds the OEHR and is insensitive to inhibition of the IR (Valzania et al., 2019; Vogel et al., 2015). However, OEH increased detection of pAKT and pERK in the ovaries and pelts (Fig. 8A and B). In the gut, OEH treatment also resulted in increased detection of pAKT in one of our biological replicates but not in two others, which resulted in our statistical analysis not detecting a

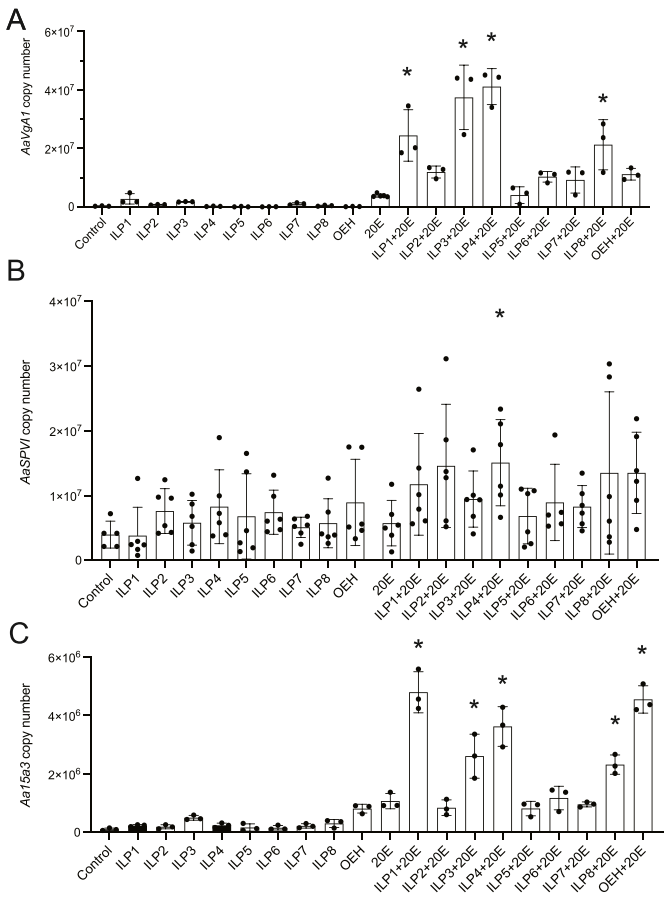

Fig. 5. ILPs and OEH with 20E differentially affect expression of *VgA1*, *SpVI*, and *15a3* in different organs. ILPs or OEH plus 20E differentially increase transcript abundance of: (A) *AaVgA1* in the fat body/pelt, (B) *AaSpVI* in the gut, and (C) *Aa15a3* in the ovaries. Pelts with fat body and ovaries were separately collected from 4-day old previtellogenic females while guts were collected from 4-day old females 1 h PBM. Each organ was placed in Sf900 II medium and treated with saline (Control), 20 pmol of ILP1-8, 20 pmol of OEH or 10 pmol of 20E alone versus each ILP or OEH plus 20E. Transcript abundance per ng of total RNA for each gene was determined 6 h post-treatment. Each bar shows treatment means ± standard deviation (SD) while solid circles indicate values for individual biological replicates. For each graph, an asterisk above a bar indicates the treatment differed from the control while no asterisk indicates the treatment did not differ (Dunnett's post-hoc multiple comparison test; P ≤ 0.05).

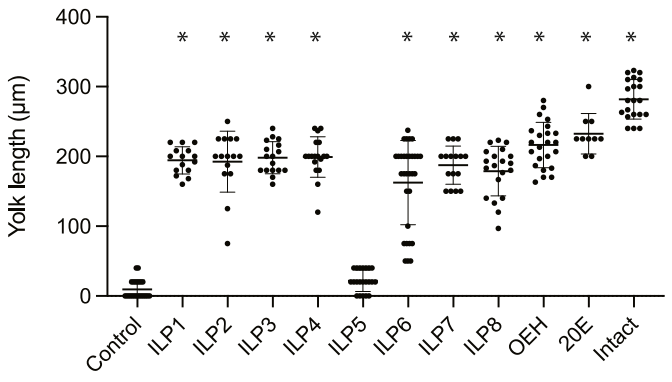

Fig. 6. Most ILPs, OEH and 20E stimulate yolk deposition into oocytes. Four-day old females were decapitated 1 h PBM and injected with saline (Control), ILP1-8 (20 pmol), OEH (20 pmol) or 20E (200 pmol). Intact females were blood fed but not decapitated. Yolk length was measured 48 h post-treatment. Each scatter plot shows treatment means ± standard deviation (SD) with solid circles indicating the yolk in oocytes for each female as measured by length. An asterisk above a given treatment indicates yolk length significantly differed from the control while no asterisk indicates the treatment did not differ (Dunnett's post-hoc multiple comparison test; P ≤ 0.05).

significant increase in pAKT signal (Fig. 8C). In contrast, pERK was detected in pelt and gut cultures in the absence of adding OEH as observed in the ILP assays (Fig. 8B and C).

4. Discussion

In this study, we first compared tissue expression patterns among *ilps* and *oeh* since differences could play a role in why certain family members have functions that differ from others during the previtellogenic and vitellogenic phases. Our results corroborate earlier findings indicating *ilp1, 3, 4, 7, 8* and *oeh* are specifically expressed in the head, *ilp5* and *ilp6* are primarily expressed in the abdomen likely either in ganglia or fat body respectively as are their homologs in *Drosophila* (Chowański et al., 2021; Nässel and Vanden Broeck, 2016; Semaniuk et al., 2021a, 2021b), while *ilp2* is primarily expressed in the ovaries (Ling and Raikhel, 2021; Riehle et al., 2006). All of the ILP family members are upregulated after blood feeding as noted for ILP3 in *Aedes albopictus* (Dai et al., 2023). However, our results also indicate patterns of expression in the previtellogenic and vitellogenic phases are largely similar among the brain-specific ILPs which suggest all similarly respond at the RNA level to sugar and blood feeding. That all ILPs are expressed during a gonadotrophic cycle is also consistent with each being detected in circulation (Ling and Raikhel, 2021). While results from this study indicate *oeh* and all *ilps* except *ilp5* are upregulated after blood feeding, only a few differences in timing of upregulation were noted. We thus conclude most ILPs and OEH have functions during the previtellogenic and vitellogenic phases, which is consistent with the *ir*, *oehr*, and *lgr4* also being expressed in all tissues that have functions in egg formation.

High level of expression of the *ir* and *oehr* in the ovaries is consistent with the essential role ILPs and OEH have in activating primary follicles, ecdysteroid production by follicle cells, synthesis of yolk proteins by the fat body that are packaged into oocytes, and chorion formation (Brown et al., 2008; Dhara et al., 2013; Valzania et al., 2019). Increased copy number of the *oehr* in ovaries by 2 h PBM suggests upregulated expression of this receptor may be important for OEH-induced synthesis of ecdysteroids, whereas the increase in transcript abundance for the *ir* at 24 h PBM could have roles in yolk packaging, chorion formation, and secondary follicle maturation, which enables females to mature eggs after consuming another blood meal (Harrison et al., 2022; Riehle and Brown, 2002). In contrast, the modest alterations in transcript abundance for the *ir* and *oehr* in other tissues suggest receptor abundance is sufficient for other physiological processes involving IIS that occur during the vitellogenic phase. The very low abundance of *lgr4* in all tissues with almost no changes during the previtellogenic and vitellogenic phases circumstantially suggest this receptor is less important than the *ir* or *oehr* in regulating the physiological processes we examined in this study.

A second factor that could be important in defining the functions of different ILP family members and OEH is their release but our results do not reveal whether any are differentially released during a gonadotrophic cycle. We earlier determined that OEH is specifically produced in mNSCs (Brown and Cao, 2001), while the ILP3-specific antibody used in this study shows this ILP also localizes to mNSCs and is likely released with OEH in greater quantities from axon terminals along the anterior midgut after blood feeding. We hypothesize the other ILPs that are specifically expressed in the head are also produced in mNSCs but confirming this and determining whether each is also concurrently released with ILP3 after blood feeding will require further study using antibodies that distinguish between family members. Several factors including 20E, JH, and serotonin have been implicated in regulating *ilp* expression in *A. aegypti* (Ling et al., 2017; Ling and Raikhel, 2018, 2021),

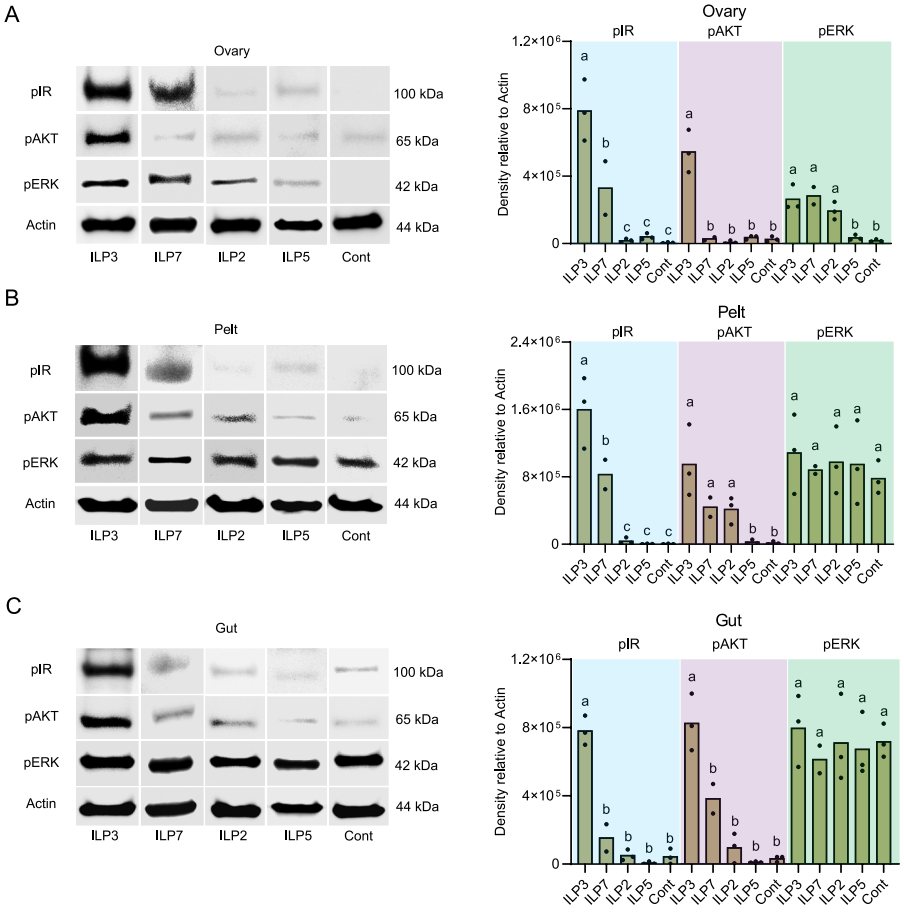

Fig. 7. ILPs differentially induce IIS in different organs. ILPs differentially induce IIS in: (A) ovaries, (B) pelts and (C) guts. Each organ was placed in *ex vivo* culture. Ovary and pelt extracts were prepared 1 h after adding 20 pmol of ILP3, 7, 2, 5 or saline only (Cont) while guts extracts were prepared 3 h after adding each ILP or saline. Immunoblots sequentially probed with antibodies to pIR, pAKT pERK, or actin (loading control) are shown to the left with molecular mass of each target protein indicated in kDa. Quantification of band intensity from three independent biological replicates are shown in graphs to the right with bars indicating mean intensity while solid circles show values for each replicate. Different letters above a bar indicate band intensity significantly differs (Tukey-Kramer post-hoc multiple comparison test; $P \leq 0.05$).

while studies in *Drosophila* and other insects identify both neuronal pathways and nutrient status through signals relayed by the fat body in stimulating ILP release from neurosecretory cells (Agrawal et al., 2016; Géminard et al., 2009; Liessem et al., 2023; Masumura et al., 2000; Park et al., 2014; Rajan and Perrimon, 2012; Sano et al., 2015). Whether these or other factors regulate the release of ILP3 and other family members in *A. aegypti* after sugar or blood feeding is an important but unanswered question.

The third factor that could play role in differential functions among ILP family members and OEH is how they interact with the IR and OEHR respectively and downstream processes affecting biological activity. In this regard, the largest weakness in the study of mosquitoes and other insects is the limited information on the biological activity and receptor binding activities of different ILP family members. As earlier noted, indirectly assessing biological activity through loss of function assays is difficult due to the large number of ILPs many insects produce and the potential for functional redundancy. However, producing each ILP has also previously not been done for any insect because structural complexity makes synthesis or expression more difficult than most other peptide hormones (Grönke et al., 2010; Nässel et al., 2015; Teleman, 2010). The novel contribution of this study is that we produced all of the *A. aegypti* ILPs and OEH. We produced ILP6 as a single chain recombinant peptide because of its predicted processing into an IGF-like family member (Riehle et al., 2006), whereas the other seven ILPs were synthesized as separate A and B chains followed by disulfide bridge formation because each is predicted to be insulin/relaxin-like (Brown et al., 2008; Riehle et al., 2006). We then used previously established *in vivo* and *ex vivo* assays to compare biological activities of each ILP and OEH in processes that are known to be required for egg formation (Dhara et al., 2013; Vogel et al., 2015). We also included JH and 20E in some of these assays because the former also has functions in nutrient storage while the latter is required for vitellogenesis (Dou et al., 2023; Gulia-Nuss et al., 2011; He et al., 2021; Hou et al., 2015; Roy et al., 2007; Wang et al., 2017; Zhu and Noriega, 2016).

During the previtellogenic phase, our results suggest only ILP8 and OEH stimulate equivalent levels of TAG storage as ILP3, while several family members expressed in the head plus ILP2 and ILP6 stimulate glycogen storage to similar or greater levels as our positive control. Broadly consistent with these results, knockout of *ilp8* in *A. aegypti* reduced TAG but not glycogen stores, while knockout of *ilp7* reduced glycogen but not TAG stores (Ling et al., 2017). However, all ILP family members are also detected in hemolymph of previtellogenic females at similar concentrations (~1–60 pg/ml) (Ling and Raikhel, 2021) to what we injected into head-ablated females in the *in vivo* assay we used (~50 pg per female). Exogenous insulin has also been shown to activate JH release in *A. aegypti* females suggesting an additional role for one or more ILPs in regulating JH titers (Hernández-Martinez et al., 2007; Hernández-Martínez et al., 2015; Perez-Hedo et al., 2013, 2014) while

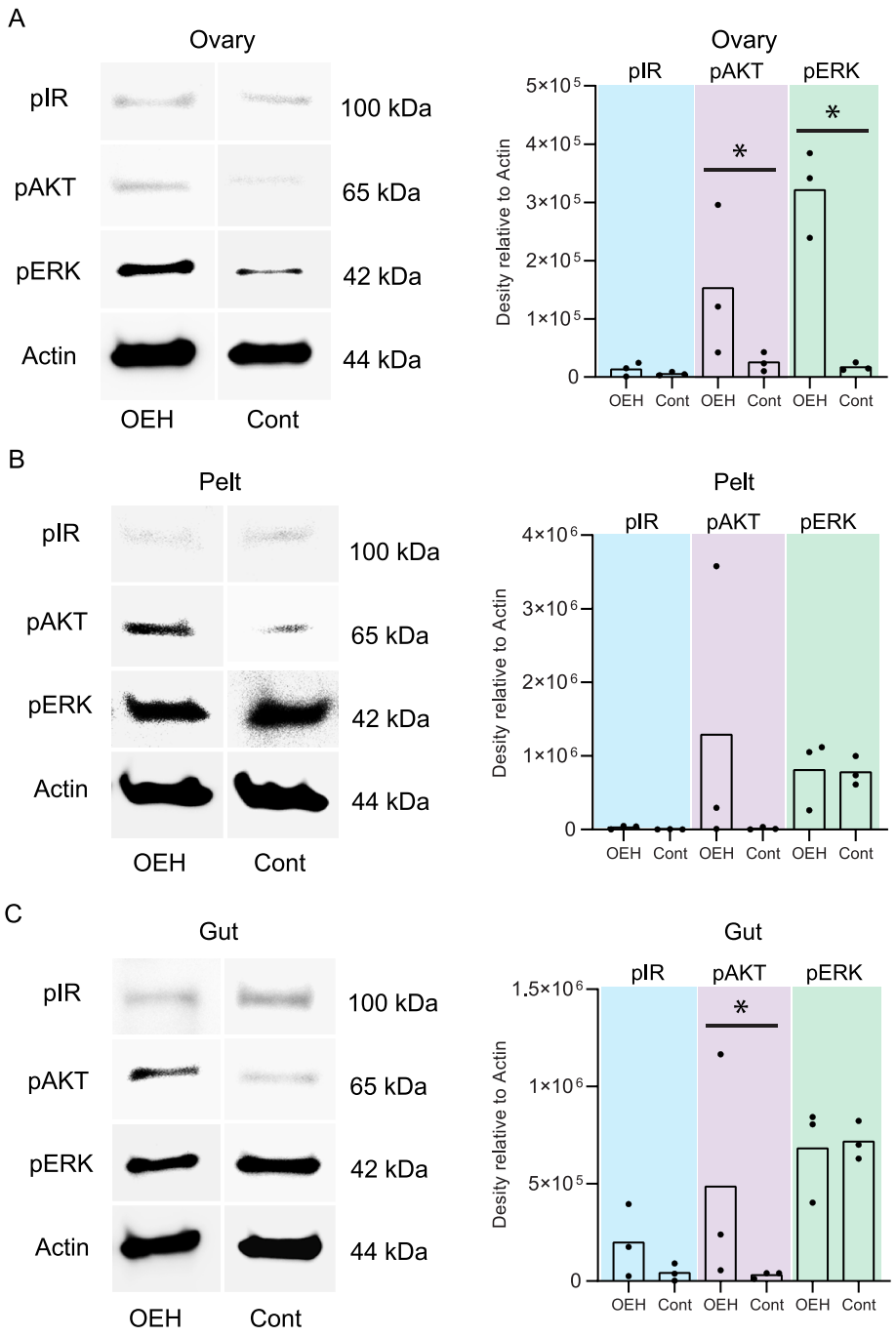

Fig. 8. OEH differentially induces IIS in different organs. OEH differentially induces IIS in: (A) ovaries, (B) pelts and (C) guts. Each organ was placed in *ex vivo* culture and extracts prepared followed by immunoblotting as described in Fig. 7. Quantification of band intensity from three independent biological replicates is shown in the graph to the right. Bars indicate mean intensity while solid circles show values for each replicate. For each treatment and target protein, an asterisk indicates band intensity significantly differed between OEH and the control sample while no asterisk indicates no difference (t- or Kruskal Wallis test; $P \leq 0.05$).

results reported here and previously indicate JH promotes nutrient storage in response to sugar and blood feeding (Dou et al., 2023). Thus, why knockout of ILP8 or ILP7 reduced TAG and glycogen stores respectively in earlier studies (Ling et al., 2017) is unclear when: 1) all ILP family members plus JH are in circulation in previtellogenic females, and 2) several ILPs and JH stimulate TAG and glycogen storage in the gain of function assays we conducted. One possibility is family members like ILP8 or ILP7 affect the expression and/or release of other family members which has precedent in studies from *Drosophila* where some ILP family members affect the release of other ILP family members (Nässel and Vanden Broeck, 2016). However, we conclude from our assays that two ILPs plus OEH can stimulate TAG storage while most ILP family members can stimulate glycogen storage by the fat body.

Activation of primary follicles and associated ecdysteroid biosynthesis is the first step after blood feeding that activates the vitellogenic phase, which is followed by Vg biosynthesis by the fat body, blood meal digestion by the midgut, and chorion deposition around oocytes after yolk packaging (Dou et al., 2023; Harrison et al., 2022; Ling et al., 2017; Roy et al., 2007). Our approach of using *ex vivo* assays allowed us to assess the biological activity of each ILP and OEH in the absence of other family members or potential interactions between the ovaries, fat body and gut. Two key findings come from these experiments. First, only

brain-specific ILPs and OEH activate ecdysteroid production by the ovaries. Second, only a subset of head-expressed ILPs (ILP1, ILP3, ILP4, and ILP8) increase transcript abundance of *AaVgA1* in the fat body, only ILP4 upregulates transcript abundance of *AaSPVI* in the gut, and all brain-specific ILPs and OEH increase transcript abundance of *Aa15-a3* in the ovaries but only if the tissues are co-cultured with 20E. These findings are fully consistent with earlier assays indicating a synergistic interaction between 20E, ILP, and TOR signaling in stimulating Vg expression and blood meal digestion (Gulia-Nuss et al., 2011; Harrison et al., 2022; He et al., 2021; Roy et al., 2007) but additionally indicate several brain-specific family members exhibit overlapping biological activities. Given only the brain-specific ILPs plus 20E stimulates *AaVgA1* expression *ex vivo*, we expected only the brain-specific family members to stimulate yolk packaging into oocytes but instead all ILPs except ILP5 did so along with OEH and 20E alone. Thus, it is again possible that ILPs and/or OEH from the head potentially affect expression and/or release of family members like ILP2 from the ovaries and ILP6 from the fat body. ILP7 is the most structurally conserved of the ILPs in *A. aegypti*, *Drosophila*, and other insects, and recent studies suggest *Drosophila* ILP7 activates LGR3 or LGR4 signaling and plays an important role in female fertility (Castellanos et al., 2013; Imambocus et al., 2022; Prince et al., 2021). However, results from this study indicate *A. aegypti* ILP7 stimulates ecdysteroid biosynthesis by the ovaries along with all of the other head-produced family members and OEH. In contrast, the absence of biological activity by ILP5 in any of the physiological processes we studied suggests either this family member is an LGR ligand or lacks biological activity because of an error in synthesis that renders it non-functional.

We conducted signaling assays with four ILPs and OEH that exhibited different biological activities because studies from vertebrates indicate insulin, IGFs and insulin analogs differentially phosphorylate the IR, which can also result in differential phosphorylation of downstream proteins and functional phenotypes (Glendorf et al., 2012; Humphrey et al., 2013; Sciacca et al., 2010; Shymko et al., 1997; Siddle, 2012; Vinayagam et al., 2016). We selected ILP3 for study because this family member activated most of the physiological processes we studied. We then compared ILP3 to ILP7 because it is another brain-specific family member that stimulated ecdysteroid biosynthesis but did not upregulate expression of *AaVgA1, AaSPVI* or *Aa15A3*. We also examined ILP2 and ILP5 because of their overall lack of activity in the biological assays we conducted. The main finding from these assays is that ILP3 exhibited the strongest activation of signaling in each tissue as measured by phosphorylation of the IR, AKT and ERK while ILP5 exhibited the least, which also correlated with the former activating several physiological processes while the latter did not. That ILP7 increased pIR, pAKT and/or pERK in the ovaries and fat body suggests this family member is an IR ligand although it could also potentially activate signaling through LGRs that we did not assess (Imambocus et al., 2022; Shymko et al., 1997). Our finding that OEH had no effect on phosphorylating the IR but increased pAKT and pERK in the ovaries is also consistent with its biological activity and prior evidence that it stimulates IIS through binding to the OEHR (Dhara et al., 2013; Vogel et al., 2015). However, we also recognize limitations in the signaling data we generated. First, we only conducted time course assays with ILP3 which we used to select time points for study when comparing phosphorylation of the IR, AKT and ERK to ILP7, ILP2 and ILP5. Thus, the incubation times we selected were potentially not optimal for OEH and the other ILPs we tested. Second, *ex vivo* culture conditions with the fat body appear to stimulate phosphorylation of ERK given we detected no pERK at 0 h in our time course study with ILP3 but strongly detected pERK after 20 min in the no ILP or OEH negative controls in our assays. Culture conditions also potentially contributed to detection of pERK in the no ILP or OEH gut cultures. Third, many other proteins in addition to the IR, AKT and ERK are phosphorylated in response to ILPs (Glendorf et al., 2012; Nässel et al., 2015; Post et al., 2018). Thus, other signaling factors than we examined could affect biological activity. While we earlier measured binding kinetics of ILP3 to the IR in the ovaries (Wen et al., 2010), an important goal going forward is to determine receptor-binding kinetics for the other ILP family members.

In summary -, our study significantly advances prior knowledge by producing all of the ILPs produced by the same species of insect (*A. aegypti*), and generating a data set that compares biological activity across several physiological processes. While some family members exhibit redundant biological activities, others do not which suggests overall activity spectra likely differ among family members due to differential interactions with the IR and potentially LGR4. Our results also indicate OEH and some ILP family members exhibit overlapping biological activities but other ILP family members do not. Lastly, our results provide evidence for different ILP family members and OEH differentially activating IIS downstream of receptor binding that potentially underlies differential biological activities in specific tissues with functions in egg formation.

Author contributions

M.R.B and M.R.S. conceived the study. K.C., X. D, M.R.B, M.R.S. designed the experimental work. K.C., X.D., J.H.H., R.A.H., M.R.B, M.R.S. performed, processed and analyzed data. M.R.S. wrote the initial draft. All authors made contributions to generating the figures, tables and editing the manuscript.

Funding

Support for the study comes from NIH R01 AI033108 (MRB, MRS), USDA Department of Agriculture Hatch Project GEO00772 (MRS) and the Pulliam Endowment (MRS). REH was also partially supported by NIH T32AI060546.

Data availability

All data are available as e-material.

Declaration of competing interest

The authors declare that the research was conducted in the absence of any commercial or financial relationships that could be construed as a potential conflict of interest.

Acknowledgements

We thank J. A. Johnson and L. South for assistance with rearing of the insects used in the study.

Appendix A. Supplementary data

Supplementary data to this article can be found online at https://doi.org/10.1016/j.ibmb.2023.104028.

References

Agrawal, N., Delanoue, R., Mauri, A., Basco, D., Pasco, M., Thorens, B., Léopold, P., 2016. The *Drosophila* TNF Eiger Is an adipokine that acts on insulin-producing cells to mediate nutrient response. Cell Metabol. 23, 675–684. https://doi.org/10.1016/j.cmet.2016.03.003.

Álvarez-Rendón, J.P., Murillo-Maldonado, J.M., Riesgo-Escovar, J.R., 2023. The insulin signaling pathway a century after its discovery: sexual dimorphism in insulin signaling. Gen. Comp. Endocrinol. 330, 114146 https://doi.org/10.1016/j.ygcen.2022.114146.

Antonova, Y., Arik, A.J., Moore, W., Riehle, M.R., Brown, M.R., 2012. Insulin-like peptides: structure, signaling, and function. In: Gilbert, L.I. (Ed.), Insect Endocrinology. Elsevier, New York, pp. 63–92. https://doi.org/10.1016/B978-0-12-384749-2.10002-0.

Bai, H., Kang, P., Tatar, M., 2012. *Drosophila* insulin-like peptide-6 (dilp6) expression from fat body extends lifespan and represses secretion of *Drosophila* insulin-like

peptide-2 from the brain. Aging Cell 11, 978–985. https://doi.org/10.1111/acel.12000.
Bathgate, R.A., Halls, M.L., van der Westhuizen, E.T., Callander, G.E., Kocan, M., Summers, R.J., 2013. Relaxin family peptides and their receptors. Physiol. Rev. 93, 405–480. https://doi.org/10.1152/physrev.00001.2012.
Baredo, E., DeGennaro, M., 2020. Not just from blood: mosquito nutrient acquisition from nectar sources. Trends Parasitol. 36, 473–484. https://doi.org/10.1016/j.pt.2020.02.003.
Belfiore, A., Malaguarnera, R., Vella, V., Lawrence, M.C., Sciacca, L., Frasca, F., Morrione, A., Vigneri, R., 2017. Insulin receptor isoforms in physiology and disease: an updated view. Endocr. Rev. 38, 379–431. https://doi.org/10.1210/er.2017-00073.
Briegel, H., 2003. Physiological bases of mosquito ecology. J. Vector Ecol. 28, 1–11.
Brown, M.R., Clark, K.D., Gulia, M., Zhao, Z., Garczynski, S.F., Crim, J.W., Suderman, R. J., Strand, M.R., 2008. An insulin-like peptide regulates egg maturation and metabolism in the mosquito *Aedes aegypti*. Proc. Natl. Acad. Sci. U.S.A. 105, 5716–5721. https://doi.org/10.1073/pnas.0800478105.
Brown, M.R., Cao, C., 2001. Distribution of ovary ecdysteroidogenic hormone I in the nervous system and gut of mosquitoes. J. Insect Sci. 1, 3. https://doi.org/10.1093/jis/1.1.3.
Cao, C., Brown, M.R., 2001. Localization of an insulin-like peptide in brains of two flies. Cell Tissue Res. 304, 317–321. https://doi.org/10.1007/s004410100367.
Castellanos, M.C., Tang, J.C., Allan, D.W., 2013. Female-biased dimorphism underlies a female-specific role for post-embryonic Ilp7 neurons in *Drosophila* fertility. Development 140, 3915–3926. https://doi.org/10.1242/dev.094714.
Chowański, S., Walkowiak-Nowicka, K., Winkiel, M., Marciniak, P., Urbanski, A., Pacholska-Bogalska, J., 2021. Insulin-like peptides and cross-talk with other factors in the regulation of insect metabolism. Front. Physiol. 12, 701203 https://doi.org/10.3389/fphys.2021.701203.
Clements, A.N., 2012. The Biology of Mosquitoes, Vol. 1: Development, Nutrition, and Reproduction. CABI, New York.
Clements, A.N., Potter, S.A., Scales, M.D.C., 1985. The cardiacal neurosecretory system and associated organs of an adult mosquito, *Aedes aegypti*. J. Insect Physiol. 30, 821–830. https://doi.org/10.1016/0022-1910(85)90075-7.
Dai, Y., Ding, J., Liang, Z., Guo, R., Yi, T., Zhu, Y., Chen, S., Liang, S., Liu, W., 2023. Molecular and expression characterization of insulin-like signaling in development and metabolism of *Aedes albopictus*. Parasites Vectors 16, 134. https://doi.org/10.1186/s13071-023-05747-8.
Dhara, A., Eum, J.H., Robertson, A., Gulia-Nuss, M., Vogel, K.J., Clark, K.D., Graf, R., Brown, M.R., Strand, M.R., 2013. Ovary ecdysteroidogenic hormone functions independently of the insulin receptor in the yellow fever mosquito, *Aedes aegypti*. Insect Biochem. Mol. Biol. 43, 1100–1108. https://doi.org/10.1016/j.ibmb.2013.09.004.
Dou, X., Chen, K., Brown, M.R., Strand, M.R., 2023. Multiple endocrine factors regulate nutrient mobilization and storage in *Aedes aegypti* during a gonadotrophic cycle. Insect Sci. 30, 425–442. https://doi.org/10.1111/1744-7917.13110.
Dzaki, N., Ramli, K.N., Azlan, A., Ishak, I.H., Azzam, G., 2017. Evaluation of reference genes at different developmental stages for quantitative real-time PCR in *Aedes aegypti*. Sci. Rep. 7, 43618 https://doi.org/10.1038/srep43618.
Géminard, G., Arquier, N., Layalle, S., Bourouis, M., Slaidina, M., Delanoue, R., Bjordal, M., Ohanna, M., Ma, M., Colombani, J., Léopold, P., 2009. Control of metabolism and growth through insulin-like peptides in *Drosophila*. Diabetes 55, S5–S8. https://doi.org/10.2337/db06-S001.
Glendorf, T., Knudsen, L., Stidsen, C.E., Hansen, B.F., Hegelund, A.C., Sørensen, A.R., Nishimura, E., Kjeldsen, T., 2012. Systematic evaluation of the metabolic to mitogenic potency ratio for B10-substituted insulin analogues. PLoS One 7, e29198. https://doi.org/10.1371/journal.pone.0029198.
Gulia-Nuss, M., Robertson, A.E., Brown, M.R., Strand, M.R., 2011. Insulin-like peptides and the target of rapamycin pathway coordinately regulate blood digestion and egg maturation in the mosquito *Aedes aegypti*. PLoS One 6, e20401. https://doi.org/10.1371/journal.pone.0020401.
Grönke, S., Clarke, D.F., Broughton, S., Andrews, T.D., Partridge, L., 2010. Molecular evolution and functional characterization of *Drosophila* insulin-like peptides. PLoS Genet. 6, e1000857 https://doi.org/10.1371/journal.pgen.1000857.
Haeusler, R.A., McGraw, T.E., Accili, D., 2018. Biochemical and cellular properties of insulin receptor signalling. Nat. Rev. Mol. Cell Biol. 19, 31–44. https://doi.org/10.1038/nrm.2017.89.
Harrison, R.E., Chen, K., South, L., Lorenzi, A., Brown, M.R., Strand, M.R., 2022. Ad libitum consumption of protein- or peptide-sucrose solutions stimulates egg formation by prolonging the vitellogenic phase of oogenesis in anautogenous mosquitoes. Parasites Vectors 15, 127. https://doi.org/10.1186/s13071-022-05252-4.
Harrison, R.E., Brown, M.R., Strand, M.R., 2021. Whole blood and blood components from vertebrates differentially affect egg formation in three species of anautogenous mosquitoes. Parasites Vectors 14, 1–19. https://doi.org/10.1186/s13071-021-04594-9.
He, Y.Z., Ding, Y., Wang, X., Zou, Z., Raikhel, A.S., 2021. E93 confers steroid hormone responsiveness of digestive enzymes to promote blood meal digestion in the midgut of the mosquito *Aedes aegypti*. Insect Biochem. Mol. Biol. 134, 103580 https://doi.org/10.1016/j.ibmb.2021.103580.
Hernández-Martinez, S., Mayoral, J.G., Li, Y., Noriega, F.G., 2007. Role of juvenile hormone and allatotropin on nutrient allocation, ovarian development and survivorship in mosquitoes. J. Insect Physiol. 53, 230–234. https://doi.org/10.1016/j.jinsphys.2006.08.009.
Hernández-Martínez, S., Rivera-Perez, C., Nouzova, M., Noriega, F.G., 2015. Coordinated changes in JH biosynthesis and JH hemolymph titers in *Aedes aegypti* mosquitoes. J. Insect Physiol. 72, 22–27. https://doi.org/10.1016/j.jinsphys.2014.11.003.
Hou, Y., Wang, X.L., Saha, T.T., Roy, S., Zhao, B., Raikhel, A.S., Zou, Z., 2015. Temporal coordination of carbohydrate metabolism during mosquito reproduction. PLoS Genet. 11, e1005309 https://doi.org/10.1371/journal.pgen.1005309.
Humphrey, S.J., Yang, G., Yang, P., Fazakerley, D.J., Stöckli, J., Yang, J.Y., James, D.E., 2013. Dynamic adipocyte phosphoproteome reveals that Akt directly regulates mTORC2. Cell Metabol. 17, 1009–1020. https://doi.org/10.1016/j.cmet.2013.04.010.
Imambocus, B.N., Zhou, F., Formozov, A., Wittich, A., Tenedini, F.M., Hu, C., Sauter, K., Macarenhas Varela, E.M., Heredia, F., Casimiro, A.P., Macedo, A., Schlegel, P., Yang, C., Miguel-Aliage, I., Wiegert, J.S., Pankratz, M.J., Gontijo, A.M., Cardona, A., Soba, P., 2022. A neuropeptidergic circuit gates selective escape behavior of *Drosophila* larvae. Curr. Biol. 32, 149–163. https://doi.org/10.1016/j.cub.2021.10.069.
Irwin, D.M., 2021. Evolution of the insulin gene: changes in gene number, sequence, and processing. Front. Endocrinol. 12, 649255 https://doi.org/10.3389/fendo.2021.649255.
Isoe, J., Rascón Jr., A.A., Kunz, S., Miesfeld, R.L., 2009. Molecular genetic analysis of midgut serine proteases in *Aedes aegypti* mosquitoes. Insect Biochem. Mol. Biol. 39, 903–912. https://doi.org/10.1016/j.ibmb.2009.10.008.
Kannan, K., Fridell, Y.W.C., 2013. Functional implications of *Drosophila* insulin-like peptides in metabolism, aging, and dietary restriction. Front. Physiol. 4, 288. https://doi.org/10.3389/fphys.2013.00288.
Kim, J., Neufeld, T.P., 2015. Dietary sugar promotes systemic TOR activation in *Drosophila* through AKH-dependent selective secretion of Dilp3. Nat. Commun. 6, 6846. https://doi.org/10.1038/ncomms7846.
Lawrence, M.C., 2021. Understanding insulin and its receptor from their three-dimensional structures. Mol. Metabol. 52, 101255 https://doi.org/10.1016/j.molmet.2021.101255.
Li, J.S., Li, J., 2006. Major chorion proteins and their crosslinking during chorion hardening in *Aedes aegypti* mosquitoes. Insect Biochem. Mol. Biol. 36, 954–964. https://doi.org/10.1016/j.ibmb.2006.09.006.
Liao, S., Nässel, D.R., 2020. *Drosophila* insulin-like peptide 8 (DILP8) in ovarian follicle cells regulates ovulation and metabolism. Front. Endocrinol. 11, 461. https://doi.org/10.3389/fendo.2020.00461.
Liessem, S., Held, M., Bisen, R.S., Haberkern, H., Lacin, H., Bockemühl, T., Ache, J.M., 2023. Behavioral state-dependent modulation of insulin-producing cells in *Drosophila*. Curr. Biol. 33, 449–463. https://doi.org/10.1016/j.cub.2022.12.005 e5.
Lin, X., Smagghe, G., 2019. Roles of the insulin signaling pathway in insect development and organ growth. Peptides 122, 169923. https://doi.org/10.1016/j.peptides.2018.02.001.
Ling, L., Kokoza, V.A., Zhang, C., Aksoy, E., Raikhel, A.S., 2017. MicroRNA-277 targets insulin-like peptides 7 and 8 to control lipid metabolism and reproduction in *Aedes aegypti* mosquitoes. Proc. Natl. Acad. Sci. U.S.A. 114, E8017–E8024. https://doi.org/10.1073/pnas.1710970114.
Ling, L., Raikhel, A.S., 2021. Cross-talk of insulin-like peptides, juvenile hormone, and 20-hydroxyecdysone in regulation of metabolism in the mosquito *Aedes aegypti*. Proc. Natl. Acad. Sci. U.S.A. 118, e2023470118 https://doi.org/10.1073/pnas.2023470118.
Ling, L., Raikhel, A.S., 2018. Serotonin signaling regulates insulin-like peptides for growth, reproduction, and metabolism in the disease vector *Aedes aegypti*. Proc. Natl. Acad. Sci. U.S.A. 115, E9822–E9831. https://doi.org/10.1073/pnas.1808243115.
Livak, K.J., Schmittgen, T.D., 2001. Analysis of relative gene expression data using real-time quantitative PCR and the $2-\Delta\Delta CT$ method. Methods 25, 402–408. https://doi.org/10.1006/meth.2001.1262.
Martinson, E.O., Chen, K., Valzania, L., Brown, M.R., Strand, M.R., 2022. Insulin-like peptide 3 stimulates hemocytes to proliferate in anautogenous and facultatively autogenous mosquitoes. J. Exp. Biol. 225, jeb243460. https://doi.org/10.1242/jeb.243460.
Masumura, M., Satake, S., Saegusa, H., Mizoguchi, A., 2000. Glucose stimulates the release of bombyxin, an insulin-related peptide of the silkworm *Bombyx mori*. Gen. Comp. Endocrinol. 118, 393–399. https://doi.org/10.1006/gcen.1999.7438.
McKinney, D.A., Strand, M.R., Brown, M.R., 2017. Evaluation of ecdysteroid antisera for a competitive enzyme immunoassay and extraction procedures for the measurement of mosquito ecdysteroids. Gen. Comp. Endocrinol. 253, 60–69. https://doi.org/10.1016/j.ygcen.2017.08.028.
Meola, S.M., Lea, A.O., 1972. The ultrastructure of the corpus cardiacum of *Aedes solloicitans* and the histology of the cerebral neurosecretory system of mosquitoes. Gen. Comp. Endocrinol. 18, 210–234. https://doi.org/10.1016/0016-6480(72)90208-0.
Mizoguchi, A., Okamoto, N., 2013. Insulin-like and IGF-like peptides in the silkmoth *Bombyx mori*: discovery, structure, secretion, and function. Front. Physiol. 4, 1–11. https://doi.org/10.3389/fphys.2013.00217, 1.
Nässel, D.R., Liu, Y., Luo, J., 2015. Insulin/IGF signaling and its regulation in *Drosophila*. Gen. Comp. Endocrinol. 221, 255–266. https://doi.org/10.1016/jygcen.2014.11.021.
Nässel, D.R., Vanden Broeck, J., 2016. Insulin/IGF signaling in *Drosophila* and other insects: factors that regulate production, release and post-release action of the insulin-like peptides. Cell. Mol. Life Sci. 73, 271–290. https://doi.org/10.1007/s00018-015-2063-3.
Nuss, A.B., Brown, M.R., 2018. Isolation of an insulin-like peptide from the Asian malaria mosquito, *Anopheles stephensi*, that acts as a steroidogenic gonadotropin across diverse mosquito taxa. Gen. Comp. Endocrinol. 258, 140–148. https://doi.org/10.1016/j.ygcen.2017.05.007.

Park, S., Alfa, R.W., Topper, S.M., Kim, G.E., Kockel, L., Kim, S.K., 2014. A genetic strategy to measure circulating *Drosophila* insulin reveals genes regulating insulin production and secretion. PLoS Genet. 10 (8), e1004555 https://doi.org/10.1371/journal.pgen.1004555.

Patil, N.A., Rosengren, K.J., Separovic, F., Wade, J.D., Bathgate, R.A.D., Hossain, M.A., 2017. Relaxin family peptides: structure–activity relationship studies. Br. J. Pharmacol. 174, 950–961. https://doi.org/10.1111/bph.13684.

Perez-Hedo, M., Rivera-Perez, C., Noriega, F.G., 2014. Starvation increases insulin sensitivity and reduces juvenile hormone synthesis in mosquitoes. PLoS One 9, e86183. https://doi.org/10.1371/journal.pone.0086183.

Perez-Hedo, M., Rivera-Perez, C., Noriega, F.G., 2013. The insulin/TOR signal transduction pathway is involved in the nutritional regulation of juvenile hormone synthesis in *Aedes aegypti*. Insect Biochem. Mol. Biol. 43, 495–500. https://doi.org/10.1016/j.ibmb.2013.03.008.

Post, S., Karashchuk, G., Wade, J.D., Sajid, W., De Meyts, P., Tatar, M., 2018. *Drosophila* insulin-like peptides DILP2 and DILP5 differentially stimulate cell signaling and glycogen phosphorylase to regulate longevity. Front. Endocrinol. 9, 245. https://doi.org/10.3389/fendo.2018.00245.

Prince, E., Kretzschmar, J., Trautenberg, L.C., Broschk, S., Brankatschk, M., 2021. Dilp7-producing neurons regulate insulin-producing cells in *Drosophila*. Front. Physiol. 12, 630390 https://doi.org/10.3389/fphys.2021.630390.

Rajan, A., Perrimon, N., 2012. *Drosophila* cytokine unpaired 2 regulates physiological homeostasis by remotely controlling insulin secretion. Cell 151, 123–137. https://doi.org/10.1016/j.cell.2012.08.019.

Riehle, M.A., Brown, M.R., 2002. Insulin receptor expression during development and a reproductive cycle in the ovary of the mosquito *Aedes aegypti*. Cell Tissue Res. 308, 409–420. https://doi.org/10.1007/s00441-002-0561-8.

Riehle, M.A., Fan, Y., Cao, C., Brown, M.R., 2006. Molecular characterization and developmental expression of insulin-like peptides in the yellow fever mosquito, *Aedes aegypti*. Peptides 27, 2547–2560. https://doi.org/10.1016/j.peptides.2006.07.016.

Roy, S., Saha, T.T., Zou, Z., Raikhel, A.S., 2018. Regulatory pathways controlling female insect reproduction. Annu. Rev. Entomol. 63, 489–511. https://doi.org/10.1146/annurev-ento-020117-043258.

Roy, S.G., Hansen, I.A., Raikhel, A.S., 2007. Effect of insulin and 20-hydroxyecdysone in the fat body of the yellow fever mosquito, *Aedes aegypti*. Insect Biochem. Mol. Biol. 37, 1317–1326. https://doi.org/10.1016/j.ibmb.2007.08.004.

Sano, H., Nakamura, A., Texada, M.J., Truman, J.W., Ishimoto, H., Kamikouchi, A., Nibu, Y., Kume, K., Ida, T., Kojima, M., 2015. The nutrient-responsive hormone CCHamide-2 controls growth by regulating insulin-like peptides in the brain of *Drosophila melanogaster*. PLoS Genet. 11, e1005209 https://doi.org/10.1371/journal.pgen.1005209.

Sciacca, L., Cassarino, M.F., Genua, M., Pandini, G., Le Moli, R., Squatrito, S., Vigneri, R., 2010. Insulin analogues differently activate insulin receptor isoforms and post-receptor signalling. Diabetologia 53, 1743–1753. https://doi.org/10.1007/s00125-010-1760-6.

Semaniuk, U., Piskovatska, V., Strilbytska, O., Strutynska, T., Burdyliuk, N., Vaiserman, A., Bubalo, V., Storey, K.B., Lushchak, O., 2021a. *Drosophila* insulin-like peptides: from expression to functions—a review. Entomol. Exp. Appl. 169, 195–208. https://doi.org/10.1111/eea.12981.

Semaniuk, U., Strilbytska, O., Malinovska, K., Storey, K.B., Vaiserman, A., Lushchak, V., Lushchak, O., 2021b. Factors that regulate expression patterns of insulin-like peptides and their association with physiological and metabolic traits in *Drosophila*. Insect Biochem. Mol. Biol. 135, 103609 https://doi.org/10.1016/j.ibmb.2021.103609.

Shabanpoor, F., Separovic, F., Wade, J.D., 2009. The human insulin superfamily of polypeptide hormones. Vitam. Horm. 80, 1–31. https://doi.org/10.1016/S0083-6729(08)00601-8.

Sharma, A., Nuss, A.B., Gulia-Nuss, M., 2019. Insulin-like peptide signaling in mosquitoes: the road behind and the road ahead. Front. Endocrinol. 10, 166. https://doi.org/10.3389/fendo.2019.00166.

Shymko, R.M., De Meyts, P., Thomas, R., 1997. Logical analysis of timing-dependent receptor signalling specificity: application to the insulin receptor metabolic and mitogenic signalling pathways. Biochem. J. 326, 463–469. https://doi.org/10.1042/bj3260463.

Siddle, K., 2012. Molecular basis of signaling specificity of insulin and IGF receptors: neglected corners and recent advances. Front. Endocrinol. 3, 34. https://doi.org/10.3389/fendo.2012.00034.

Smýkal, V., Pivarči, M., Provazník, J., Bazalová, O., Jedlička, P., Lukšan, O., Horák, A., Vaněčková, H., Beneš, V., Fiala, I., Hanus, R., Doležel, D., 2020. Complex evolution of insect insulin receptors and homologous decoy receptors, and functional significance of their multiplicity. Mol. Biol. Evol. 37, 1775–1789. https://doi.org/10.1093/molbev/msaa048.

Strand, M.R., Brown, M.R., Vogel, K.J., 2016. Mosquito peptide hormones: diversity, production, and function. Adv. Insect Physiol 51, 145–188. https://doi.org/10.1016/bs.aiip.2016.05.003.

Sun, J., Hiraoka, T., Dittmer, N.T., Cho, K.H., Raikhel, A.S., 2000. Lipophorin as a yolk protein precursor in the mosquito, *Aedes aegypti*. Insect Biochem. Mol. Biol. 30, 1161–1171. https://doi.org/10.1016/s0965-1748(00)00093-x.

Teleman, A.A., 2010. Molecular mechanisms of metabolic regulation by insulin in *Drosophila*. Biochem. J. 425, 13–26. https://doi.org/10.1042/BJ20091181.

Valzania, L., Coon, K.L., Vogel, K.J., Brown, M.R., Strand, M.R., 2018. Hypoxia-induced transcription factor signaling is essential for larval growth of the mosquito *Aedes aegypti*. Proc. Natl. Acad. Sci. U.S.A. 115, 457–465. https://doi.org/10.1073/pnas.1719063115.

Valzania, L., Mattee, M.T., Strand, M.R., Brown, M.R., 2019. Blood feeding activates the vitellogenic stage of oogenesis in the mosquito *Aedes aegypti* through inhibition of glycogen synthase kinase 3 by the insulin and TOR pathways. Dev. Biol. 454, 85–95. https://doi.org/10.1016/j.ydbio.2019.05.011.

Veenstra, J.A., 2020. Arthropod IGF, relaxin and gonadulin, putative orthologs of *Drosophila* insulin-like peptides 6, 7 and 8, likely originated from an ancient gene triplication. PeerJ 8, e9534. https://doi.org/10.7717/peerj.9534.

Vinayagam, A., Kulkarni, M.M., Sopko, R., Sun, X., Hu, Y., Nand, A., Villalta, C., Moghimi, A., Yang, X., Mohr, S.E., Hong, P., Asara, J.M., Perrimon, N., 2016. An integrative analysis of the InR/PI3K/Akt network identifies the dynamic response to insulin signaling. Cell Rep. 16, 3062–3074. https://doi.org/10.1016/j.celrep.2016.08.029.

Vogel, K.J., Brown, M.R., Strand, M.R., 2013. Phylogenetic investigation of peptide hormone and growth factor receptors in five dipteran genomes. Front. Endocrinol. 4, 193. https://doi.org/10.3389/fendo.2013.00193.

Vogel, K.J., Brown, M.R., Strand, M.R., 2015. Ovary ecdysteroidogenic hormone requires a receptor tyrosine kinase to activate egg formation in the mosquito *Aedes aegypti*. Proc. Natl. Acad. Sci. U.S.A. 112, 5057–5062. https://doi.org/10.1073/pnas.1501814112.

Wang, X.L., Hou, Y., Saha, T.T., Pei, G.F., Raikhel, A.S., Zou, Z., 2017. Hormone and receptor interplay in the regulation of mosquito lipid metabolism. Proc. Natl. Acad. Sci. U.S.A. 114, E2709–E2718. https://doi.org/10.1073/pnas.1619326114.

Wen, Z., Gulia, M., Clark, K.D., Dhara, A., Crim, J.W., Strand, M.R., Brown, M.R., 2010. Two insulin-like peptide family members from the mosquito *Aedes aegypti* exhibit differential biological and receptor binding activities. Mol. Cell. Endocrinol. 328, 47–55. https://doi.org/10.1016/j.mce.2010.07.003.

World Health Organization, 2014. A global brief on vector-borne diseases. https://apps.who.int/iris/handle/10665/111008.

Zhang, H., Liu, J., Li, C.R., Momen, B., Kohanski, R.A., Pick, L., 2009. Deletion of *Drosophila* insulin-like peptides causes growth defects and metabolic abnormalities. Proc. Natl. Acad. Sci. U.S.A. 106, 19617–19622. https://doi.org/10.1073/pnas.0905083106.

Zhu, J., Noriega, F.G., 2016. The role of juvenile hormone in mosquito development and reproduction. Adv. Insect Physiol 51, 93–113. https://doi.org/10.1016/bs.aiip.2016.04.005.

Ziegler, R., Ibrahim, M.M., 2001. Formation of lipid reserves in fat body and eggs of the yellow fever mosquito, *Aedes aegypti*. J. Insect Physiol. 47, 623–627. https://doi.org/10.1016/s0022-1910(00)00158-x.